Charles University in Prague
Faculty of Mathematics and Physics

DOCTORAL THESIS

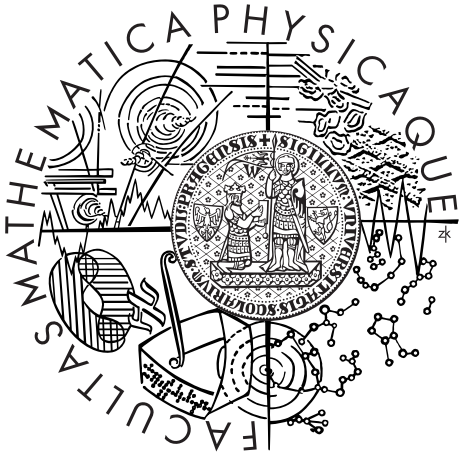

Zdeněk Švindrych

Low-field excitations in magnetite

Department of Low Temperature Physics

Supervisor of the doctoral thesis:	RNDr. Zdeněk Janů, CSc.
Study programme:	Physics
Specialization:	Physics of Condensed Matter and Materials Research

Prague 2013

I am greatly indebted to my supervisor Zdeněk Janů who has led me through the process of scientific development, has critically examined all outputs of my research and created encouraging conditions for successful completion of this thesis. I am also very thankful to my wife Zuzana who has always stood by me and was so supportive when I had hard times writing this thesis and took care of me, our children and the household when I was completely engrossed in disclosing magnetic properties of solids... My thanks also go to Helenka Štěpánková, Andrzej Kozłowski and numerous others for supplying precious samples and otherwise supporting this work.

Typeset in LaTeX.

I declare that I carried out this doctoral thesis independently, and only with the cited sources, literature and other professional sources.

I understand that my work relates to the rights and obligations under the Act No. 121/2000 Coll., the Copyright Act, as amended, in particular the fact that the Charles University in Prague has the right to conclude a license agreement on the use of this work as a school work pursuant to Section 60 paragraph 1 of the Copyright Act.

In Prague on the .....

signature of the author

Název práce: Excitace v magnetitu ve slabých polích

Autor: Zdeněk Švindrych

Katedra: Katedra fyziky nízkých teplot

Vedoucí dis. práce: RNDr. Zdeněk Janů, CSc., Katedra fyziky nízkých teplot

Abstrakt: V této práci jsou prezentovány výsledky detailních magntických a dielektrických vlastností vysoce kvalitních monokrystalických vzorků magnetitu (Fe_3O_4) ve slabém magnetickém a elektrickém poli. Tato měření mohou odhalit detaily fázových přechodů a jiných jevů, které ještě nejsou uspokojivě popsány. Soustředili jsme se nejen na tzv. Verweyův přechod - známý fázový přechod nastávající při teplotě kolem 120 K ve stechiometrických vzorcích - ale také jsme prozkoumali a popsali nové relaxační jevy v magnetitu za nízkých teplot. Také jsme zjistily vyjímečnou citlivost nízkoteplotních vlastností na kvalitě, stechiometrii a homogenitě vzorku. Výsledky prezentované v této práci byly naměřeny na citlivém nekomerčním skvidovém magnetometru a doplněny čtyřbodovou dielektrickou spektroskopií a měřením stejnosměrné vodivosti.

Klíčová slova: magnetická susceptibilita, magnetit, Verweyův přechod, SQUID, relaxace

Title: Low-field excitations in magnetite

Author: Zdeněk Švindrych

Department: Department of Low Temperature Physics

Supervisor: RNDr. Zdeněk Janů, CSc., Department of Low Temperature Physics

Abstract: We have performed detailed measurements of magnetic and dielectric properties of high quality magnetite (Fe_3O_4) single crystals in weak magnetic and electric fields. These measurements can reveal details of phase transitions and other features that are not yet fully understood. We focused not only at the Verwey transition - a well known phase transition taking place at about 120 K in stoichiometric samples - but we also explored and described new relaxation effects in magnetite at low temperatures. The low-temperature properties were also found to be exceptionally sensitive to sample quality, stoichiometry and homogeneity. The results presented in this thesis were acquired on sensitive non-commercial SQUID magnetometer complemented by four-probe dielectric spectroscopy and dc conductivity measurements.

Keywords: magnetic susceptibility, magnetite, Verwey transition, SQUID, relaxation

Contents

Introduction **3**

1 Theory and present status **5**
1.1 Magnetism . . . 5
1.1.1 Introduction . . . 5
1.1.2 Magnetic domain structure . . . 5
1.1.3 Magnetic susceptibility . . . 6
1.1.4 Demagnetising effects . . . 9
1.1.5 Debye relaxation . . . 11
1.1.6 Magnetocrystalline anisotropy . . . 13
1.2 Charge transport . . . 14
1.2.1 Metal-insulator transition . . . 14
1.2.2 Variable-range hopping model of dc electrical conductivity 15
1.2.3 Impurity ac conduction in semiconductors . . . 15
1.3 Crystal structure of magnetite . . . 16
1.3.1 Spinel structure . . . 16
1.3.2 Inverse and random spinel structures . . . 16
1.3.3 Low-temperature structure of magnetite, the Verwey transition . . . 18
1.4 The origin of magnetite samples . . . 19
1.4.1 Natural crystals . . . 19
1.4.2 Synthetic bulk crystals . . . 20
1.4.3 Thin film samples . . . 20
1.4.4 Nanocrystals and colloids . . . 20
1.5 Physical properties of magnetite . . . 20
1.5.1 General properties . . . 20
1.5.2 Effects of doping . . . 21
1.5.3 Specific heat measurements . . . 22
1.5.4 Magnetite at high pressures . . . 23
1.6 Magnetic measurements . . . 23
1.6.1 Susceptibility measurements . . . 23
1.6.2 Magnetic after-effect measurement . . . 23
1.6.3 NMR measurements . . . 25

2 Materials and Methods **27**
2.1 Samples . . . 27
2.1.1 Magnetite samples . . . 27
2.1.2 Other samples . . . 27
2.2 Magnetic measurements . . . 27
2.2.1 Force magnetometers . . . 28
2.2.2 Induction magnetometers . . . 28
2.2.3 SQUID magnetometer . . . 29
2.3 Electric transport measurements . . . 32
2.3.1 Dc conductivity measurements . . . 32
2.3.2 Ac dielectric measurements . . . 32

2.4 Temperature measurement and control 33

3 Results on stoichiometric magnetite 35
3.1 Samples overview 35
3.2 Overall ac susceptibility 35
3.3 The Verwey transition 36
3.3.1 Latent heat of the phase transition 36
3.3.2 Thermal hysteresis in magnetic measurements 37
3.3.3 Behaviour of spontaneous magnetization 39
3.3.4 Electrical conductivity 40
3.4 Glass-like transition 42
3.4.1 Magnetic ac susceptibility 42
3.4.2 Correlation with dielectric properties 44
3.5 Low-temperature anomaly 46
3.5.1 Novel relaxation phenomenon 47
3.5.2 Excitation of the anomaly 51

4 Results on doped magnetite 53
4.1 Samples overview 53
4.2 The Verwey transition 53
4.3 Glass-like transition 54
4.4 Low-temperature anomaly 56

5 Discussion 57
5.1 The Verwey transition 57
5.2 Low-temperature magnetic behaviour of magnetite 59
5.2.1 Glass-like transition 59
5.2.2 Low-temperature anomaly 61
5.3 Transport properties of magnetite below the Verwey transition . . 63
5.3.1 DC electric conductivity of magnetite 63
5.3.2 AC dielectric properties of magnetite 63

Conclusion 65

Bibliography 67

Author's publications and presentations 73

List of Symbols and Abbreviations 75

Introduction

Magnetite is a naturally occurring iron oxide with an empirical formula Fe_3O_4. The unusual physical properties of this mineral were already known in the ancient Greece and medieval China where spontaneously magnetized pieces of magnetite were used as compasses for naval navigation. It was the attraction of small pieces of iron to the magnetized mineral that was the first observation of the property of magnetism. It was also a very important ingredient in the development of modern theories of magnetism and metal-insulator transitions. In geology the conditions of magnetite formation and its ability to record the direction of magnetic field during geological changes (paleomagnetism) are still used extensively. Last but not least, the biological role of magnetite in magnetotactic bacteria, bees, pigeons and other species is studied in a great detail.

The physicist's interest in magnetite was revived in 1940's when a unique structural transition accompanied by a large change in electric conductivity was observed [69], later coined the Verwey transition. The occurrence of this transition stimulated theoretical treatment of metal-insulator transition [48, 49] and the variable-range hopping model of electrical conductivity. The magnetite has since been studied extensively in all forms, namely natural and synthetic bulk single crystals, polycrystals, powders, thin films, single-domain particles and nanoparticle colloids; and by all possible experimental techniques. The wealth of scientific knowledge gathered during the last 70 years was ordered in important topical reviews [19, 75] which form an important source of information about this compound. A notable conclusion from reviewing past experiments is the paramount importance of sample quality - most of the earlier experiments on natural samples do reflect the properties of the respective samples, but not those intrinsic to magnetite.

Despite the experimental and theoretical effort, some aspects and mechanisms behind the Verwey transition and other properties of magnetite at low temperatures have not been fully explained yet. This work aims at providing additional detailed experimental information about magnetic and dielectric properties of the highest quality synthetic single-crystalline magnetite samples subjected to weak magnetic and electric fields in temperature range from 5 K to 130 K. The high sensitivity of magnetic measurements is achieved with a SQUID magnetometer, a device where the phenomenon of magnetic flux quantisation is employed to reach extremely fine responsiveness to the changes of magnetic flux. The electric properties were probed with a precision RLC bridge (for high sensitivity ac measurements of complex impedance) and an electrometer (for measuring very low dc conductivity of magnetite at low temperatures).

One of the motivations to perform the measurements presented in this work was to try to find a relationship between the metal-insulator transition (MIT) observed in magnetite and the MITs that are known to play a role in the superconductivity of high-T_c cuprates. The suitability of magnetite is supported by the fact, that the MIT can be traversed simply by changing temperature (as opposed to cuprates, where the transition is controlled by doping). Another advantageous property of magnetite is the decoupling between charge and spin degrees of freedom, pronounced by the difference between the ferrimagnetic Neel temperature

(858 K) and the Verwey temperature (120 K).

We investigated the detailed magnetic and dielectric behaviour of magnetite at the Verwey transition and at lower temperatures and attempted to correlate the magnetic and dielectric properties with the results of other past and recent experiments. Emphasis was put on the evolution of magnetic susceptibility and spontaneous magnetic moment during the Verwey transition at $\approx$ 120 K, the temperature and frequency dependence of magnetic susceptibility and dielectric permittivity during so-called glass-like transition at 30 K - 70 K and the magnetic aspects of newly described anomalous visco-elastic relaxation-diffusion phenomenon below 30 K (also called the low-temperature magnetic anomaly). Other effects, such as non-linear magnetic behaviour in some temperature ranges, that manifests itself as an appearance of higher harmonic susceptibilities, are also discussed in this thesis.

The thesis is divided into the following parts:

- Chapter 1 (Theory and present status) summarises the existing theories and experimental knowledge concerning magnetite, mainly its structural, magnetic and dielectric properties.

- Chapter 2 (Materials and methods) explains the basic principles of measuring magnetic and dielectric properties of solids; the main methods used in this work (SQUID magnetometer, dielectric measurements) are described in greater details.

- Chapter 3 (Experimental results on stoichiometric magnetite) presents the data obtained for multiple magnetite samples - stoichiometric high quality single crystals of magnetite.

- Chapter 4 (Experimental results on non-stoichiometric magnetite) presents the data obtained for samples of single crystals of magnetite doped to some level of nonstoichiometry.

- Chapter 5 (Discussion) gives the final overview of the measured results and comparison of these results to the current theoretical predictions.

- Conclusion briefly summarizes the results and perspectives of the measurements.

- The thesis is finalised with a complete list of bibliography, list of selected author's publications and list of abbreviations and symbols used throughout the text.

1. Theory and present status

1.1 Magnetism

1.1.1 Introduction

Magnetism is an important branch of solid state physics. It describes and explains the appearance of atomic magnetic dipoles and their mutual interactions. These interactions can be described at the atomic scale (leading e.g. to magnetic ordering - ferromagnetism, ferrimagnetism and antiferromagnetism), or at the macroscopic scale (dealing e.g. with magnetic domains and demagnetising effects).

When a solid is subject to a constant or time-varying magnetic field, the response (magnetisation of the solid) depends on the type of substance and on various quantum effects taking place in the solid. We distinguish these basic categories:

- non-ordered atomic moments - several contributions to the susceptibility exist. In diamagnets the shielding effect of orbiting electrons dominates (Langevin diamagnetism). In metals the delocalised electrons present both diamagnetic (Landau) and paramagnetic (Pauli) contribution. In conventional paramagnets the individual atoms posses nonzero magnetic moment, but due to the random orientation of these moments only weak positive susceptibility results.

- ordered aromic moments - ferromagnetism (parallel arrangement of moments), antiferromagnetism (antiparallel arrangement of equal moments) and ferrimagnetism (antiparallel arrangement of unequal moments) are the most important manifestations of magnetic ordering. This thesis is devoted to the study of magnetically ordered materials.

- superconductors - their perfect diamagnetic response is caused not only by the shielding currents flowing without dissipation, but also by the Meissner effect that is based on the fact that under some conditions magnetic vortices are energetically unfavourable.

1.1.2 Magnetic domain structure

In a typical ferromagnet at temperatures well below T_C the competition between exchange interaction (that favours parallel alignment of atomic moments) and magnetic self-energy (that favours zero stray magnetic field) results in magnetic domain structure. A bulk of ferromagnet is divided by domain walls (called also Bloch walls [9]) into microscopic regions of saturated magnetisation M_S. The width δ_B and the energy γ of a 180° Bloch wall in an uniaxial material with anisotropy constant K_1 and exchange energy A are [65]

$$\delta_B = \pi\sqrt{\frac{A}{K_1}} \tag{1.1}$$

$$\gamma = 4\sqrt{AK_1}\,. \tag{1.2}$$

We see that the anisotropy (K_1) favours narrow walls to minimize the number of moments deviating from the easy axis. The exchange interaction (A), on the other hand, prefers parallel alignment of moments, i.e. small magnetisation gradients corresponding to wide wall. Typical domain wall widths (energies) are 5 nm (50 mJ/m^2) and 100 nm (0.1 mJ/m^2) for hard and soft magnetic materials, respectively.

The formation of magnetic domains is favourable when the energy cost of a domain wall formation (γ) is outweighed by the decrease of the magnetostatic energy ($\frac{1}{2}\mu_0 M_s^2$). This is true for spherical particles whose radius exceeds a *critical single-domain radius* [65]

$$R_{sd} \approx \frac{36\sqrt{AK_1}}{\mu_0 M_s^2} \ . \tag{1.3}$$

This value ranges from a few nm in soft materials to about 1 μm in hard magnets.

Due to the variety of domain patterns encountered in ferromagnets and ferrimagnets under different conditions it is difficult to estimate the magnetostatic interactions and calculate the domain sizes. This is complicated by the fact, that many competing domain structures have similar energies. Moreover, the domain structure inside the bulk of a material, generally inaccessible experimentally, differs significantly from the situation at the surface. Under certain limitations the domain structure can be studied by numerical micromagnetic simulations [62].

The magnetic domain structure of magnetite below the Verwey transition temperature (T_V) is further complicated by the structural domains that appear as a consequence of the symmetry breaking at the transition (see Section 1.3.3 below). The interplay between these two domain structures, where anisotropy and magnetostriction play dominant roles, is not yet clarified. Nevertheless, several observations of the magnetic domain structure exist [8, 29, 46]. The reported domain structure depends in a complicated manner on the sample shape and surface treatment, the average domain sizes ranging from few μm to cca 100 μm.

1.1.3 Magnetic susceptibility

The basic method of measuring magnetic properties of solids is applying some (generally time dependent) magnetic field $H_a(t)$ and observing the sample's response magnetisation $M(t)$. One type of such a measurement is the magnetisation loop, where the applied field is swept slowly across extended range, often causing saturation in the sample (see Figure 1.1). The hysteresis behaviour is represented by nonzero remanence (remaining magnetisation after the H is brought back to zero) and coercitivity (the value of H needed to bring the magnetisation to zero). This behaviour is caused by two major mechanisms: (i) nucleation of magnetic domains - this is the case of strong rare-earth magnets, such as NdFeB; and (ii) pinning of domain walls on defects of size comparable to the domain wall width - as is the case of majority magnetic systems.

Due to the hysteresis and nonlinearity of the $M(H)$ dependence the simple definition of magnetic susceptibility $\chi = M/H$ looses its sense; a more practical

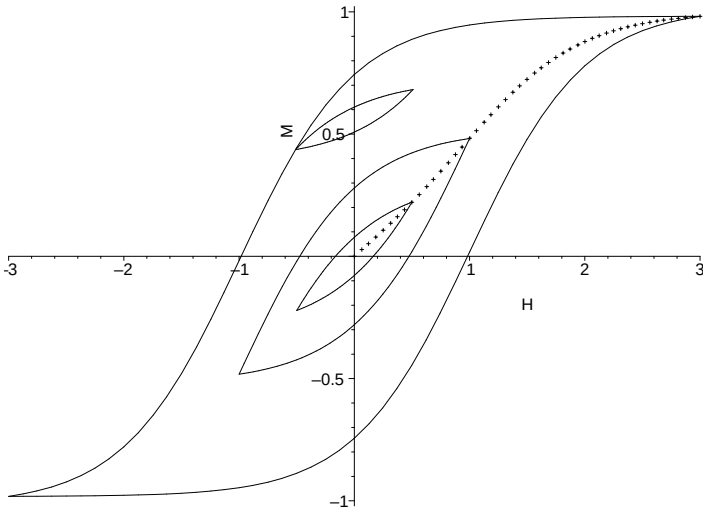

Figure 1.1: An example of a technical magnetisation loop. Shown is the virgin magnetisation curve (dotted line), first-order magnetisation loops of increasing H_{max} and a minor magnetisation loop.

approach defines χ as the local slope of $M(H)$, namely

$$\chi(H_a) = \left.\frac{\partial M}{\partial H}\right|_{H=H_a} . \tag{1.4}$$

This quantity, however, still depends on the magnitude of applied field and the history of magnetic treatment. To simplify the matter some sort of standardized conditions must be defined - most often the measurement starts in the demagnetised state, so the virgin $M(H)$ curve is followed. Often the susceptibility analysis is further simplified by assuming only weak magnetic fields, as is the case for majority of results show in this thesis, so the slope of $M(H)$ virgin curve around $H = 0$ is measured.

The differential susceptibility (Equation 1.4) is not very convenient from the experimentalist's point of view, as the measuring conditions and accompanying calculations are not well defined (an ordinary numerical differentiation introduces too much noise into the measurement). Note also the difference between the slopes of the major and minor magnetisation loops (in Figure 1.1) near the point of their contact. This is where ac susceptibility comes into consideration:

$$\chi_{ac}(H_{ac}, H_{dc}, f) = \frac{M_1(H_{ac}, H_{dc}, f)}{H_1} , \tag{1.5}$$

where H_1 is the harmonic (ac) component of the applied field H_a:

$$H_a(t) = H_0 + H_1 \cos(\omega_a t) , \tag{1.6}$$

(here the variable names H_0 and H_{dc} are used interchangeably, as well as H_1 and H_{ac}), and M_1 is the principal ac component (i.e. at the frequency of the applied field ω_a) of the sample magnetisation. This value can be conveniently (with high

precision and low noise) measured using a lock-in amplifier, or (still better) using a Fourier analysis of the measured $M(t)$ signal (provided that the sampling is synchronous with the generation of $H_a(t)$):

$$M_1 = \mathscr{F}\Big[M(t)\Big](\omega)\Big|_{\omega=\omega_a} . \tag{1.7}$$

Note, however, that the ac susceptibility (Equation 1.5) generally differs from the differential susceptibility (Equation 1.4) in three main aspects: (i) the magnitude of χ_{ac} is given by the shape of the minor $M(H)$ loop (see Figure 1.1) which may differ from the local slope of the main magnetisation loop. (ii) The $H(t)$ waveform is explicitly stated when measuring χ_{ac} and the frequency ω_a of the probing ac field appears as additional valuable parameter. Finally, (iii) differential susceptibility is (by definition) real-valued, whereas χ_{ac} (as well as M_1) is complex and represents both reactive and dissipative parts of the susceptibility.

The notion of the magnetic susceptibility can be further extended to encompass local nonlinear $M(H)$ dependence. In the case of single-valued local $M(H)$ dependence (i.e. no hysteresis) it is natural that higher orders of the expansion

$$M(H) = M_s + \chi_1 H + \chi_2 H^2 + \cdots \tag{1.8}$$

cause higher harmonics to appear (note the property of trigonometric functions, eg.: $\cos^2(\omega t) = \frac{1}{2}(\cos(2\omega t) + 1)$, that is where the second harmonic comes from). The same generalisation is valid even when the imaginary part of the harmonic susceptibilities are nonzero. This leads to generalisation of Eqs. 1.5 and 1.7 to

$$\chi_n(H_{ac}, H_{dc}, f) = \frac{M_n(H_{ac}, H_{dc}, f)}{H_1 \cdot \Big(H_1/|H_1|\Big)^{n-1}} \text{ , and} \tag{1.9}$$

$$M_n = \mathscr{F}\Big[M(t)\Big](\omega)\Big|_{\omega=n\omega_a} . \tag{1.10}$$

The denominator of Equation 1.9 contains additional phase term that ensures correct result even when the applied field has nonzero phase, as is often the case when the true value of the applied field $H_a(t)$ is sensed an processed in a similar manner to $M(t)$, namely $H_1 = \mathscr{F}[H_a(t)](\omega)|_{\omega=\omega_a}$.

It is worth noting that the energy density dissipated per cycle is proportional to the area of the magnetisation loop according to

$$\frac{E}{V} = \mu_0 \int M \mathrm{d}H = \mu_0 \int M \frac{\partial H}{\partial t} \mathrm{d}t = \mu_0 \pi H_1^2 \chi_1'' \tag{1.11}$$

$$\chi_n = \chi_n' - i \cdot \chi_n'' . \tag{1.12}$$

Namely, only the imaginary part of the first (fundamental) harmonic susceptibility χ_1'' represents dissipation; higher harmonics do not have such natural interpretation. For completeness Equation 1.12 states a common way the real and imaginary parts of susceptibilities are defined.

1.1.4 Demagnetising effects

When a homogeneous sample of finite dimensions is placed into a homogeneous magnetic field H_a, the magnetisation M (inhomogeneous in general) that develops inside the sample influences the magnetic field H_i inside the sample according to

$$H_i = H_a - DM\,, \tag{1.13}$$

where D is a demagnetising factor that depends on the sample geometry. The Equation 1.13 strictly holds only in the case of ellipsoid of revolution with the symmetry axis oriented along the applied field. In other cases the sample magnetisation is not homogeneous and Equation 1.13 must be generalised to a position-dependent vector equation. Table 1.1 summarizes the demagnetisation factors in some high-symmetry or limiting cases; more general cases can be solved numerically.

Table 1.1: A summary of exact values of demagnetisation factors in simple cases of high symmetry or limiting cases.

Geometry	Demagnetising factor
sphere	1/3
thin disc normal to field	1
thin disc parallel to field	0
long cylinder normal to field	1/2
long cylinder parallel to field	0

It is also important to consider the effect of demagnetisation on the measured susceptibility. If we define intrinsic and apparent susceptibilities χ_i and χ_a as

$$\chi_i = \frac{M}{H_i}\,,\quad \chi_a = \frac{M}{H_a}\,, \tag{1.14}$$

then Equation 1.13 can be simply expressed in terms of these susceptibilities as

$$\frac{1}{\chi_a} = \frac{1}{\chi_i} + D\,. \tag{1.15}$$

To discuss the relation between the observed and the internal susceptibility we will consider three limiting cases:

(i) $|\chi_i| \ll 1$, as is the case for weak paramagnets and diamagnets, the magnetisation M is weak and (as can be seen from Equation 1.15 and from the fact that $0 \leq D \leq 1$) the demagnetising effect can be neglected, $\chi_a \simeq \chi_i$.

(ii) $\chi_i = -1$, as is the case for superconductors, the measured susceptibility is enhanced by large screening when $D \to 1$ and diverges as $\chi_a = 1/(D-1)$.

(iii) $\chi_i \gg 1$, as is the case for ferromagnets and ferrimagnets, it follows from Equation 1.15 that the measured susceptibility is limited by demagnetisation factor, $\chi_a \leq 1/D$. However, χ_a is approaching this limit very gradually.

These aspects are shown schematically in Figure 1.2, where the the $\chi_a(\chi_i)$ dependence is drawn for several values of the demagnetising factor D. In particular, the third case is important in our measurements and prevents us from measuring the susceptibility variations when the susceptibility is very high, namely $\chi_i \gg 1/D$. For susceptibilities of the order of 10^3 the required sample shape is rather impractical and such measurements are more conveniently performed on a toroidal sample that act as the core of a transformer [64].

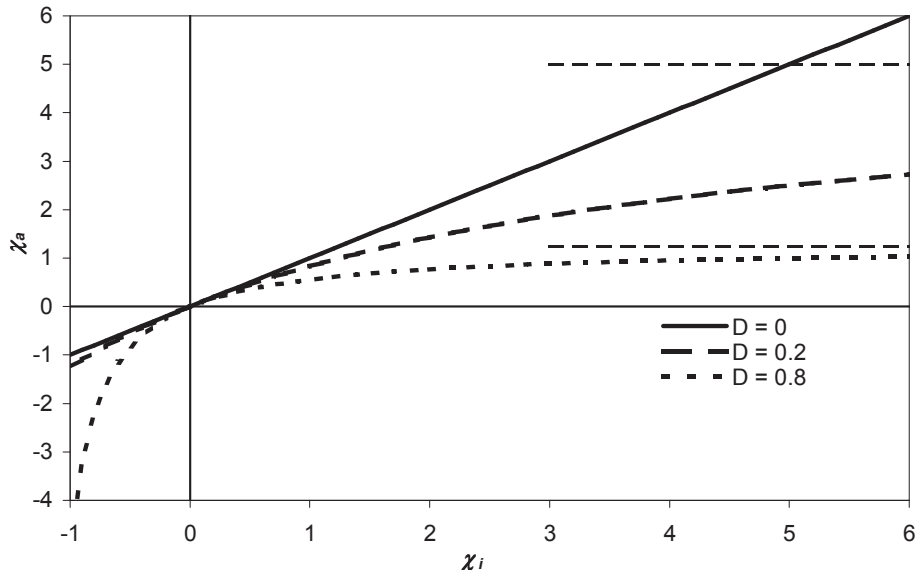

Figure 1.2: A plot of the effect of nonzero demagnetising factor on the observed susceptibility. Three curves represent increasing demagnetising factor, namely 0, 0.2 and 0.8; the thin dashed lines indicate the limiting values for the two latter cases.

The results of the preceding paragraphs remain valid even for other useful definitions of susceptibility, namely the differential susceptibility (as defined in Equation 1.4) and complex ac susceptibility (as defined in Equation 1.5 and subsequent equations). The latter case, which is particularly relevant for the results presented in this work, is indeed surprisingly complicated. Not only is the Equation 1.15 complicated by assuming complex susceptibilities, also nonlinear $M(H)$ dependence brings about higher harmonics of susceptibility that intermix in a complicated manner when one transforms between χ_a and χ_i. In that case an applied field H_a of the simple form of Equation 1.6 produces an internal field H_i that already contains higher harmonics; a general response to pure harmonic internal field cannot be calculated from the measured susceptibilities. There are three main approaches to simplification of this problem:

(i) $D \simeq 0$: this trivial assumption naturally leads to the conclusion that the measured complex ac harmonic susceptibilities equal the intrinsic values, namely $\chi_{i,n} \simeq \chi_{a,n}$.

(ii) Linear $M(H)$ dependence: because both the demagnetising effect (Equation 1.13) and Fourier transform are linear, rather simple relation between $\chi_{i,1}$ and $\chi_{a,1}$ is expected and higher harmonic susceptibilities equal zero.

However, as detailed in the Section 1.1.5 devoted to a simple linear model of Debye relaxation, some caution and detailed calculation is necessary (in the mentioned model a nonzero demagnetisation leads to non-trivial shift of the transition frequency).

(iii) Quasistatic (time independent, generally nonlinear) case: the experimental time t (that appears in the $H_a \approx \cos(\omega t)$) can be monotonously transformed into time t' in which $H_i \approx \cos(\omega t')$, although H_i would contain higher harmonics in the original time t representation. In this transformed time axis the measured data may be processed (by Fourier transform) to yield the $\chi_{i,n}$ values. This, however, can only be performed numerically and there is no simple correspondence between the $\chi_{i,n}$ and $\chi_{a,n}$ values, as the harmonics mix in a complicated way. In respect of all these difficulties the description of the material magnetic properties by means of complex ac harmonic susceptibilities is not particularly suitable.

In the most general case - nonlinear time dependent $M(H)$ response - the $t \to t'$ time transformation cannot be performed and the intrinsic $\chi_{i,n}$ values would only be accessible by dynamically adjusting the $H_a(t)$ waveform to yield pure harmonic $H_i(t)$ dependence. This approach is technically challenging and the results are not worth the effort.

1.1.5 Debye relaxation

Debye relaxation is a very simple linear model that provides complex (delayed in time) response to a harmonic applied field. It is often used to describe various transitions in dielectrics and it will also be used to analyse a specific transition in magnetite (the "glass-like transition", see Section 3.4). The Debye model is based on the relaxation time approximation that assumes the driving force (magnetic field) acts upon magnetic moments whose response is described by a single relaxation time:

$$\frac{\mathrm{d}M(t)}{\mathrm{d}t} = -\frac{M(t)}{\tau} + kH(t) \,, \tag{1.16}$$

where τ is the characteristic relaxation time and k is a constant related to the susceptibility of the moments M to the applied field H.

The solution to the linear differential Equation 1.16 can be conveniently found by introducing pure harmonic $M(t)$ and $H(t)$ dependences, more specifically

$$M(t) = M_1 \mathrm{e}^{i\omega t} \,, H(t) = H_1 \mathrm{e}^{i\omega t} \,, \tag{1.17}$$

where M_1 and H_1 are complex amplitudes in general. With a help of few symbolic manipulations and new definitions of $\omega_0 = 1/\tau$ and $\chi_1 = k\tau$ one arrives at the Debye's susceptibility

$$\chi_D = \frac{M_1}{H_1} = \chi_1 \frac{1}{1 + i\frac{\omega}{\omega_0}} \,. \tag{1.18}$$

This result can be further generalised by assuming another group of moments, that are freely movable even at the highest frequencies and cause an offset susceptibility χ_0:

$$\chi_D = \frac{M_1}{H_1} = \chi_0 + \chi_1 \frac{1}{1 + i\frac{\omega}{\omega_0}} \,, \tag{1.19}$$

whose frequency dependence is depicted in Figure 1.3. Note, that the χ_0 term can be naturally obtained from the underlying differential Equation 1.16 if a term proportional to $\mathrm{d}H(t)/\mathrm{d}t$ is added to this equation.

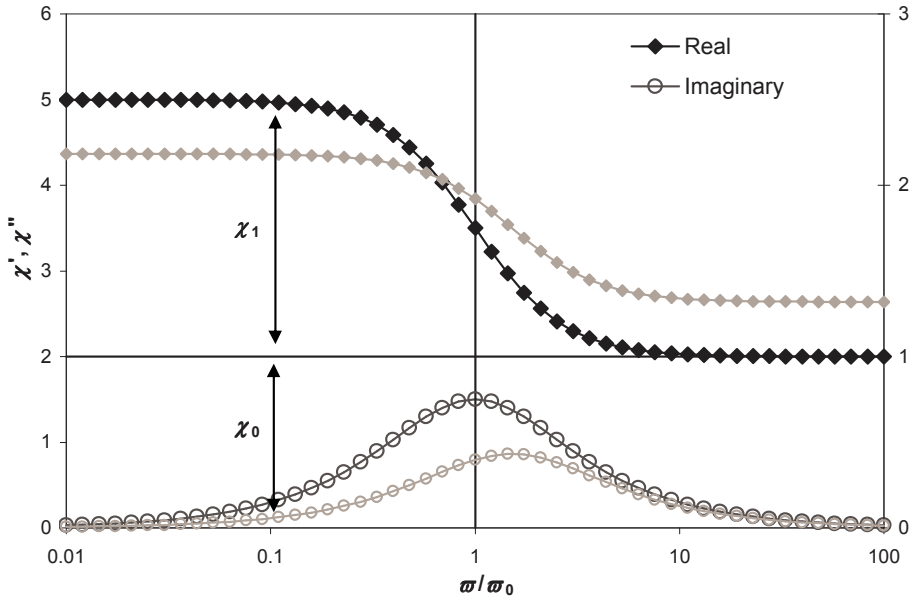

Figure 1.3: A plot of the real and imaginary part of ac susceptibility of the Debye's relaxation (black symbols) and the apparent susceptibility caused by demagnetisation ($D = 0.26$, gray symbols, right axis). The shift of the transition is clearly visible. Note the logarithmic frequency axis. The height of the peak of the imaginary part is equal to $\chi_1/2$.

Let's now consider the effect of demagnetisation, as described in the Section 1.1.4, on the internal and apparent susceptibility. Either by substituting demagnetisation Equation 1.13 into Debye's differential Equation 1.16 and solving as described above, or by substituting Debye susceptibility (Equation 1.19) into the susceptibility relation 1.15 (this approach is justified, because both Debye relaxation and demagnetisation are linear in H and M), one arrives at an expression that again has the form of Equation 1.19. This should be less of a surprise if one realises the importance of the above mentioned linearity. If one assumes intrinsic Debye's transition of the form

$$\chi_{i,D} = \chi_{i,0} + \chi_{i,1}\frac{1}{1 + i\frac{\omega}{\omega_{i,0}}} , \tag{1.20}$$

then the effect of nonzero demagnetisation factor D will cause the observed (apparent) Debye's transition to follow the equation

$$\chi_{a,D} = \chi_{a,0} + \chi_{a,1}\frac{1}{1 + i\frac{\omega}{\omega_{a,0}}} \tag{1.21}$$

with the following transformation of constants:

$$\begin{aligned}
\chi_{a,0} &= \frac{\chi_{i,0}}{1+\chi_{i,0}D} \\
\chi_{a,1} &= \frac{\chi_{i,0}+\chi_{i,1}}{1+(\chi_{i,0}+\chi_{i,1})D} - \chi_{a,0} \\
\omega_{a,0} &= \omega_{i,0}\left(1+\frac{\chi_{i,1}D}{1+\chi_{i,0}D}\right) ,
\end{aligned} \tag{1.22}$$

thus not only the susceptibilities are diminished by the demagnetising effect, but also the transition frequency is shifted - a result important for the analysis of glass-like transition in magnetite (see Section 3.4).

It is important to realise that in general any transition, that is manifested by change of susceptibility or magnetisation, will experience a shift (in frequency, temperature, etc.) caused by nonzero demagnetising effect. The shift will be larger for more gradual transitions; the shape of the transition is generally not preserved.

1.1.6 Magnetocrystalline anisotropy

Magnetocrystalline anisotropy is the dependence of the internal energy of a magnetic solid on the direction of magnetisation with respect to the crystalline lattice of the solid. It arises mainly from spin-orbit coupling, a quantum-mechanical interaction between the electron's spin and the magnetic field generated by it's orbital motion (and the orbital momentum of the electrons on neighbouring lattice sites).

The anisotropy is generally expressed as a power series in the direction cosines of magnetisation. The magnitudes and signs of the coefficients of expansion then determine special directions termed as easy or hard axes (planes), i.e. directions along which the anisotropy energy reaches its lowest or highest value respectively.

Various measurements of magnetocrystalline anisotropy of magnetite as a function of temperature are summarised in Figure 1.4. The data illustrate a dramatic change of magnetocrystalline anisotropy during the Verwey transition. Due to the lower symmetry of magnetite below T_V, new anisotropic constants appear, and some of them quite large. We also briefly note an *isotropic point* at about 130 K, where the main cubic component passes zero and the magnetic susceptibility reaches extremely large values [64].

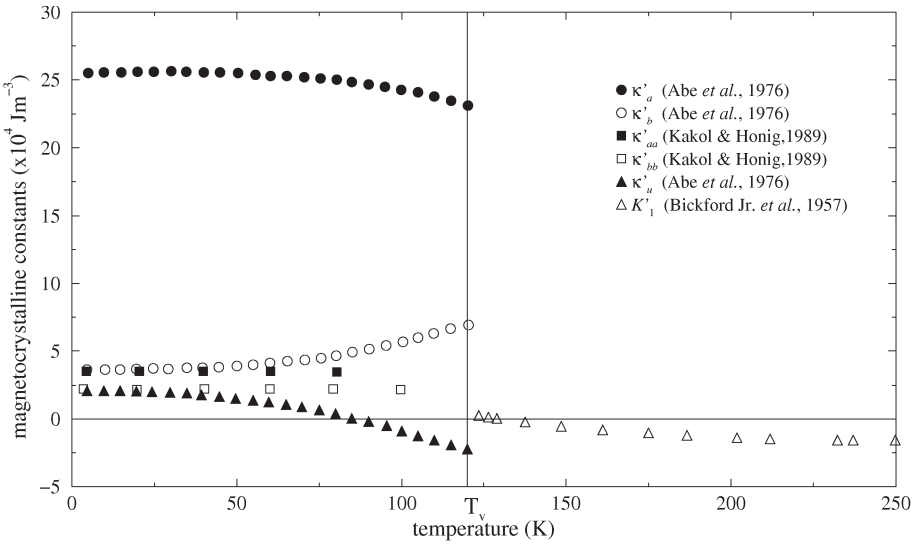

Figure 1.4: Temperature dependence of anisotropic constants of magnetite above and below the Verwey transition. Above T_V the cubic anisotropic constant K_1 is rather small, where as below T_V monoclinic anisotropic constants appear, and some of them quite large (e.g. K_a). Adapted after [51], sources: [7, 28, 33].

1.2 Charge transport

1.2.1 Metal-insulator transition

According to classical band-structure theory of solids the distinction between metals and insulators lies in the Fermi level with respect to the band structure. If the Fermi level lies in a band gap (e.g. transition metal compounds with filled d-shells) the material is an insulator (or a semiconductor, if the band-gap is not very large); on the other hand, transition metal compounds with half-filled d-shells are predicted to be metals, as the Fermi level lies in the conduction band. This is however in contradiction with many compounds, such as NiO, which is insulating even though the d-shell of nickel is partially filled. Mott (see [49] for a review) was first to address this issue theoretically, by considering electron-electron correlation effects, that may lead to electron localisation and destruction of the metallic conductivity.

Several manifestations of Mott's metal-insulator transition (MIT) were observed, e.g. by varying the lattice constant (induced by external pressure), by varying the doping of a semiconductor or by inducing disorder (Anderson's localisation model [3]). The same theory was also applied to the Verwey transition in magnetite, where the low conductivity below T_V is explained as an electron localisation, or equivalently stated, charge ordering among Fe^{3+} and Fe^{2+} sites in the mixed-state oxide. However, both theoretical and experimental aspects of this charge-ordering process still need to be fully elucidated.

1.2.2 Variable-range hopping model of dc electrical conductivity

The proposed charge localisation in magnetite also led to the model of charge transport in such a system, namely the Mott's variable-range hopping (VRH) model [50]. It is distinct from other models, such as Arrhenius' temperature activation, by its temperature dependence:

$$\sigma_{dc}(T) = \sigma_0 \mathrm{e}^{(-T_0/T)^{1/4}} \ . \tag{1.23}$$

Many authors have tried to apply this model to the experimental data of magnetite conductivity below T_V [32, 61, 74] with a limited success, as they could only fit a small temperature range of the $\sigma(T)$ dependence, or identified several temperature regions on which they could fit their experimental data to Equation 1.23.

1.2.3 Impurity ac conduction in semiconductors

A simple model of hopping ac conduction in the Debye approximation with single relaxation constant τ leads to a frequency dependence of [4]:

$$\sigma'_{ac} \approx \omega^2\tau/(1+\omega^2\tau^2) \ . \tag{1.24}$$

However, experimental data often suggest almost linear $\sigma(\omega)$ relationship [17]. Such relationship can be obtained if one generalises Equation 1.24 by assuming a distribution $n(\tau)$ of random relaxation times acting in parallel and independently. This leads to

$$\sigma'_{ac} \approx \int_0^\infty n(\tau) \frac{\omega^2\tau}{(1+\omega^2\tau^2)} \ , \tag{1.25}$$

and by plugging a specific distribution (e.g. $1/\tau^s$) one immediately arrives at $\sigma \approx \omega^s$. As the low-frequency limit of Equation 1.24 gives $\sigma \approx \omega^2$ dependence, the exponent value is constrained to $s < 2$. In most disordered physical systems $s < 1$ [56]. Temperature dependence is then introduced through $\tau(T)$ (or $n(\tau, T)$) dependence. The "ω^s" model requires quite broad distribution of relaxation times, so the temperature dependence is expected to be rather weak.

More elaborate models do exist, as well as models that aim at combining the experimental ac and dc conductivities. The simplest one would be a simple additive model according to Equation 1.26:

$$\begin{aligned} \sigma'(\omega) &= \sigma'_{ac}(\omega) + \sigma_{dc} \ , \\ \sigma''(\omega) &= \sigma''_{ac}(\omega) \ , \end{aligned} \tag{1.26}$$

where σ_{dc} is e.g. the Mott's VRH conductivity (see Equation 1.23) and $\sigma'_{ac}(\omega)$ and $\sigma''_{ac}(\omega)$ are the real and imaginary part of ac conductivity according to the relaxation model (note that the conductivity and permittivity are not independent, but $\sigma = \mathrm{i}\omega\varepsilon$, thus $\sigma''(\omega) = \omega\varepsilon'(\omega)$).

More elaborate theories, such as percolation theories combined with tunnelling between disordered states [12] naturally replicate the Mott's semi-empirical $T^{1/4}$ relation in the dc limit; at the same time they correspond well with experimental ac conductivities of various disordered systems.

1.3 Crystal structure of magnetite

1.3.1 Spinel structure

Magnetite belongs to cubic point group of symmetry at room temperature. However, the atomic arrangement is quite complicated, as the elementary unit cell contains 8 Fe_3O_4 units (a total of 56 atoms) arranged in so-called spinel structure (see Figure 1.5).

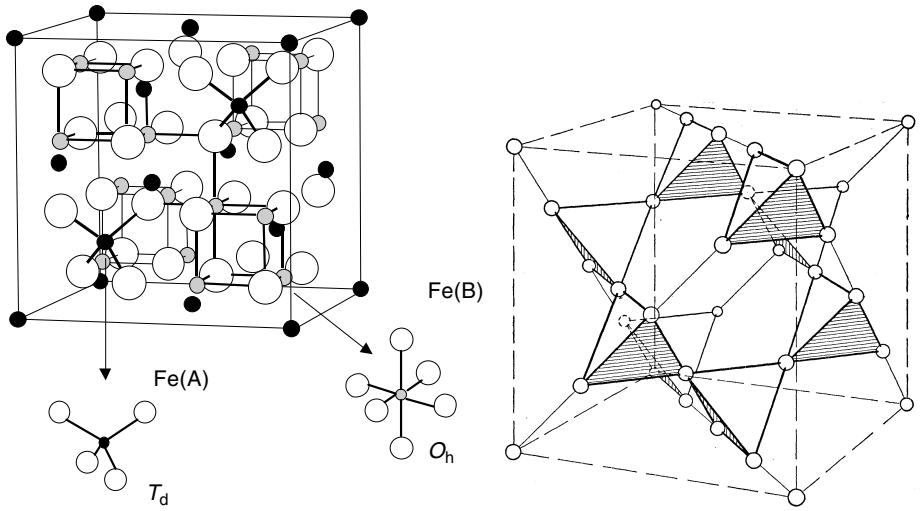

Figure 1.5: A schematic view of the structure of magnetite. Left: a cubic unit of magnetite with tetrahedra Fe ions (back spheres), octahedral Fe ions (gray spheres) and oxygen ions (white spheres). Right: the lattice of octahedral sites in spinel. Adapted from [19] and [2].

Spinels are cubic minerals of the general form AB_2O_4, where A and B are usually metals in oxidation states 2+ and 3+ respectively. As ionic compounds these are usually (with the exception of magnetite) poor electric and thermal conductors.

The complicated structure can be simplified by realizing that various metal ions occupy two types of symmetry positions: 8 tetrahedral positions and 16 octahedral positions. In a properly ordered spinel the tetrahedral positions are occupied by the A^{2+} ions. In the following sections we will term the electrons of the reaction $A^{2+} \leftrightarrow A^{3+} + e^-$ as "free" electrons; although they are usually strongly bound to their A^{2+} ions (and thus are not quite free), they can be free in the case of magnetite...

1.3.2 Inverse and random spinel structures

In the special case of magnetite, where both A and B are Fe ions (that only differ in their charges) different cation distributions appear. At very high temperatures (about 1400 K) the eight free electrons (those that form the Fe^{2+} ions in the unit cell) are randomly distributed over 24 Fe ions, thus there are on average 8/3 Fe^{2+} ions in the tetrahedral positions and 16/3 Fe^{2+} ions in the octahedral positions - so called random spinel [43, 45], see Figure 1.6.

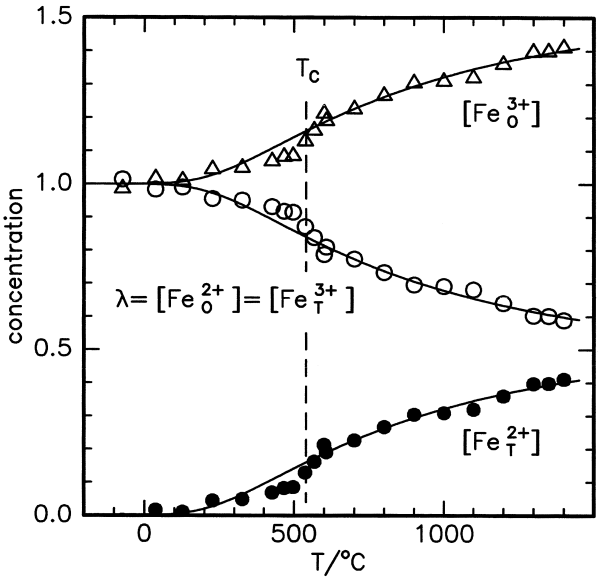

Figure 1.6: A temperature dependence of degree of inversion in magnetite at elevated temperatures as determined from Mossbauer spectra. It shows that at room temperature and below the electrons in magnetite are distributed such as to form a pure inverse spinel, whereas at about 1500 K the electrons are distributed randomly. Adapted from [43].

With decreasing temperature the thermal excitations are insufficient to keep this random distribution and at room temperature an *inverse spinel* is formed. In this configuration the tetrahedral positions are occupied exclusively by Fe^{3+} ions (hence the name "inverse"; in a normal spinel only Fe^{2+} ions would appear here), and the octahedral positions are occupied by equal amounts of Fe^{2+} and Fe^{3+} ions. In other words, the eight free electrons (per unit cell) are distributed among the 16 octahedral positions in random, dynamic and even delocalised manner.

As a matter of fact, it is this distribution (or ordering) of these free electrons among octahedral Fe ions that is at the heart of the high electrical conductivity of magnetite, the Verwey transition, and the puzzle for scientist over the last several decades.

The Fe ions in magnetite have nonzero spin moments which are ordered ferrimagnetically below the Néel temperature (around 860 K). The tetrahedral and octahedral sublattices are oriented antiparallel, the moments of Fe^{3+} ions cancel and the total magnetic moment (per unit cell) comes from eight Fe^{2+} ions. A theoretical value of 4 μ_B (per formula unit) corresponds well to the experimental value of 4.1 μ_B below room temperature, see Figure 1.7. Notably, the value of saturated magnetization is insensitive to the distribution of electrons among the octahedral sites and does not change abruptly at T_V [53].

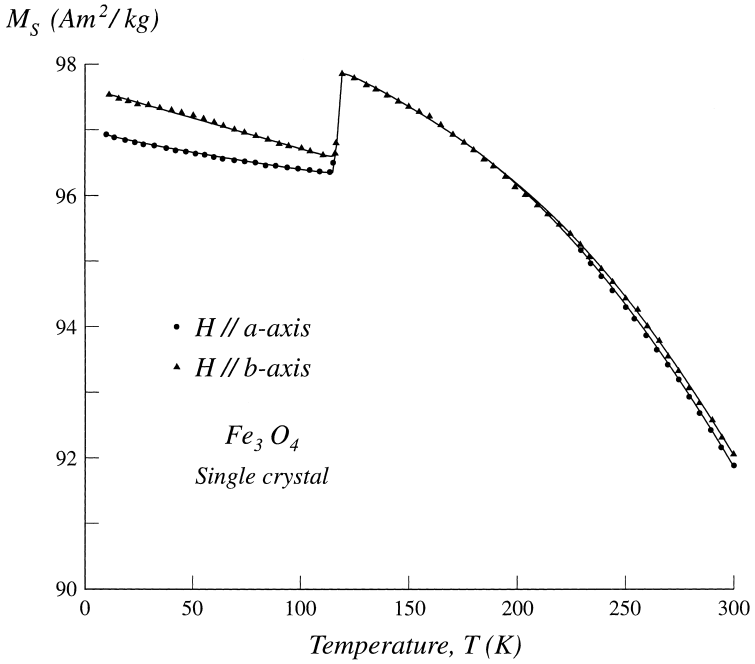

Figure 1.7: The saturated magnetisation M_s of magnetite during cooling from 300 K to 10 K in a field $H_a = 2$ T along a and b axis. The $M_s(T)$ is similar, except the jump at T_V is almost indiscernible (not shown). Adapted from [53].

1.3.3 Low-temperature structure of magnetite, the Verwey transition

More than ten years before Verwey's original work, the structural transition of magnetite at 120 K was identified by Parks and Kelly [55] as a specific heat anomaly. Several low-temperature crystal symmetries were proposed during following decades (tetragonal, rhomboedric, monoclinic, triclinic). Nowadays, the crystal symmetry is generally assumed to be monoclinic Cc, as was determined by x-ray diffraction [63, 78] and NMR [52]. Other measurements, however, suggest even lower crystal symmetry (magnetoelectric measurements [58], appearance of ferroelectricity [30] and x-ray topography measurements [46]). The low-symmetry unit cell is related to the original cubic cell (of dimension a) in the following way (see Figure 1.8): the new **a** and **b** vectors are mutually perpendicular face diagonals of the original cubic cell ($[1\bar{1}0]$ and $[110]$, thus have a length of $a\sqrt{2}$), and the **c** vector has a length of $2a$ and points in the $[001]$ direction.

The Verwey transition, called after E. J. W. Verwey, is one of the most intriguing features of magnetite. The most prominent feature of this transition is a two-order decrease of electrical conductivity when a high-quality magnetite sample is cooled through the transition [69]. The transition is also accompanied by a large increase of magnetic anisotropy (and subsequently a large decrease of mangetic susceptibility) [54] and more or less random changes of magnetisation. Verwey has also proposed a microscopic model of the transition to explain the observed transport properties. The Verwey model is an ionic order-disorder transition: above T_V the electrons can move freely among the octahedral ions, whereas below T_V a static ordered pattern of Fe^{2+} and Fe^{3+} ions is established

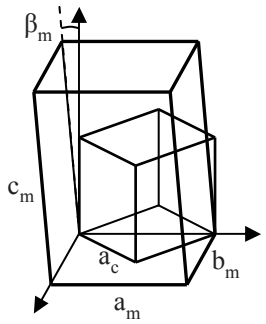

Figure 1.8: A schematic illustration of the relationship between the high-temperature cubic phase unit cell and the monoclinic unit cell of the low-temperature phase of magnetite.

that does not support conduction. Despite seven decades of effort such ordering has not yet been unambiguously proven experimentally.

Critical to interpreting magnetic measurements is the understanding of domain structure of magnetite. Above T_V a single cubic crystal is divided into magnetic domains (of size about 30 μm [8]) to lower the energy associated with stray magnetic field, and any of the equivalent [001] is an easy axis. At about 130 K the easy axis switches to [110] (and equivalents), the magnetic susceptibility rises to a very high value (in the order of 10^3 [64]) and the magnetisation of individual domains rotates to the new easy directions. At T_V, however, the crystal symmetry is reduced significantly and only the c axis of the new structure is the easy axis. As a result of competition of the structural instability and magnetostatic energy the crystal divides into structural domains, each having its c axis parallel to the local magnetisation direction.

1.4 The origin of magnetite samples

1.4.1 Natural crystals

Although as soon as in 1913 Renger [76] used synthetic magnetite samples, most of the early studies were performed on natural crystals. A somewhat 'mythic' belief in the natural crystals being optimal material for research prevailed well into 1950s, when it was already clear that sample quality is of paramount importance and the natural samples, depending on their origin, varied widely in structure, stoichiometry, impurity content, etc. (see also the effects of deliberate doping in Section 1.5.2). This habit has also introduced numerous uncertainities and contradictions into the field, which were later difficult to eradicate.

In modern research only high quality synthetic crystals are regarded as a valuable source of knowledge; the natural magnetite being studied only in the fields of geology and Earth and planetary science.

A completely different class of natural magnetite samples are single domain nanocrystals found naturally in some magnetotactic bacteria and in the brains of several species, such as bees or pigeons. These are interesting from different points of view and will not be covered in this work.

1.4.2 Synthetic bulk crystals

Over the years, two techniques established as being able to produce high quality samples with low concentration of defects, high homogeneity and precisely controlled stoichiometry and impurity content: skull melter technique and floating zone technique. To further enhance the sample quality or to modify the oxygen stoichiometry the samples can be annealed in various atmospheres.

In the skull melter technique [22] the central region of a mass of sintered pure Fe_2O_3 powder is melted by rf waves, oxidised and equilibrated in a controlled atmosphere of CO/CO_2. During gradual cooling of the melt the atmosphere composition is adjusted to maintain desired level of stoichiometry. This is a crucible-less method in a sense that the crucible is not in contact with the melt but a layer of sintered iron oxide isolates the melt.

In the floating zone technique [10] a portion of the starting ceramic material is heated by a focused radiation from a xenon arc lamp. As the material is shifted through the active zone it recrystallizes as a purified monocrystal. Further annealing is required to obtain samples of desired stoichiometry.

1.4.3 Thin film samples

Thin films of magnetite can be grown on appropriate substrates (e.g. Si, MgO, Al_2O_3) by various techniques, such as evaporation [18], reactive sputtering [44], pulsed laser deposition [21] or molecular beam epitaxy [40]. The samples are either polycrystals or single crystals with considerable tensile stress and their properties, although being very interesting, are not quite identical to that of high quality bulk single crystals. Namely, the Verwey transition is observed only in some cases, the change of electrical conductivity during the transition is not so substantial and the effects at low temperatures (glass-like transition and the low-temperature magnetic anomaly) were not reported.

1.4.4 Nanocrystals and colloids

Apart from the above mentioned biogenous magnetite nanocrystals, some effort was put into the study of properties of synthetic nanocrystals and colloids of magnetite nanoparticles. Magnetite powders may be prepared simply by grinding a bulk polycrystalline material. To prepare crystal in the nanometer range a different approach is used, usually a coprecipitation of Fe^{2+} and Fe^{3+} in a solution [38, 57]. These reactions usually produce magnetite colloids (ferrofluids) that can be stabilised by appropriate surface treatment of the nanoparticles. Again, the Verwey transition is hard to observe in such materials and the effects at low temperatures (glass-like transition and the low-temperature magnetic anomaly) were not reported.

1.5 Physical properties of magnetite

1.5.1 General properties

Spinels are cubic crystals, optically opaque at visible wavelengths (i.e. they are black), they are usually electrical insulators (or large bandgap semiconductors)

and many are magnetically ordered at room temperature. The exceptional property of magnetite among other spinels is its high (almost metallic) electrical conductivity at room temperature even in its purest crystalline form. Other general properties of magnetite are listed in Table 1.2. Properties that are strongly temperature dependent (such as magnetic susceptibility, electrical conductivity) are not listed. Omitted are also properties as coercitivity and remanence, as they depend critically on sample purity and microstructure.

Table 1.2: A summary of general physical properties of magnetite. Values specified at room temperature, unless noted otherwise. Sources: [19, 59, 75].

property	symbol	value	unit	note
formula		Fe_3O_4		
lattice constant	a	0.8394	nm	cubic
density	ϱ	$5.2 \cdot 10^3$	kg/m^3	
molar mass	m_M	231.6	g/mol	
space group $T > T_V$		$Fd3m$		cubic
space group $T < T_V$		Cc		monoclinic
Neel temperature	T_N	850	K	
saturated magnetisation	M_s	92	Am^2/kg	
refractive index	n	2.42		
Vickers hardness	VHN_{100}	≈ 750	kg/mm^2	natural
speed of sound	v_p	7100	m/s	longitudinal
bulk modulus	K	185	GPa	natural

1.5.2 Effects of doping

A very important feature of magnetite is the strong dependence of its low-temperature propeties on the level of impurities or nonstoichiometry. More specifically, the character and temperature of the Verwey transition are extremely sensitive to departure from stoichiometry (see Figure 1.9). When the stoichiometry parameter δ of $Fe_{3(1-\delta)}O_4$ exceeds a critical value $\delta_c = 0.0039$ [19] the Verwey transition changes from first order do second order, and for δ above $3\delta_c$ the transition disappears. Similar effect can be produced by doping with certain ions, such as Ti^{4+} or Zn^{2+} [35].

From these findings it is clear, that sample quality and homogeneity is of utmost importance. The use of poorly controlled or even natural magnetite samples has led to many confusions, such as multistage Verwey transitions and others. The quality control is even more important in the case of doped samples, as, for example, introducing larger amounts of ion vacancies requires quenching of the sample at the end of the annealing process.

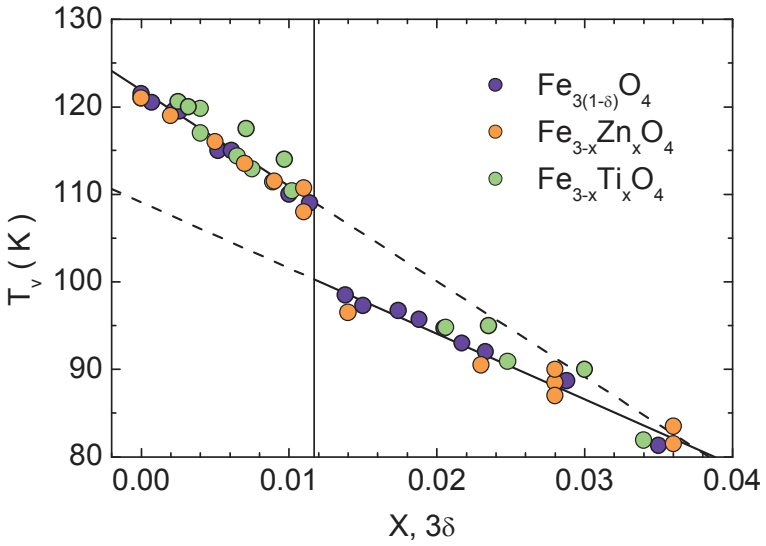

Figure 1.9: A plot of experimental dependence of the Verwey transition temperature on the level of doping or nonstoichiometry. Adapted from [35] and personal communication with A. Kozlowski.

1.5.3 Specific heat measurements

One of the first measurements indicating a phase transition in magnetite at low temperatures were specific heat measurements by Parks and Kelly [55]. They noticed an excess transformation heat in the region of 113 to 117 K; however they concluded that this temperature is too low for a structural phase transition, a view that soon changed dramatically. Some of the first results are illustrated in Figure 1.10. Since then, numerous investigations of the specific heat anomaly associated with the transition were performed in order to elucidate whether the transition is of first or second order. A throughout summary is provided in [34].

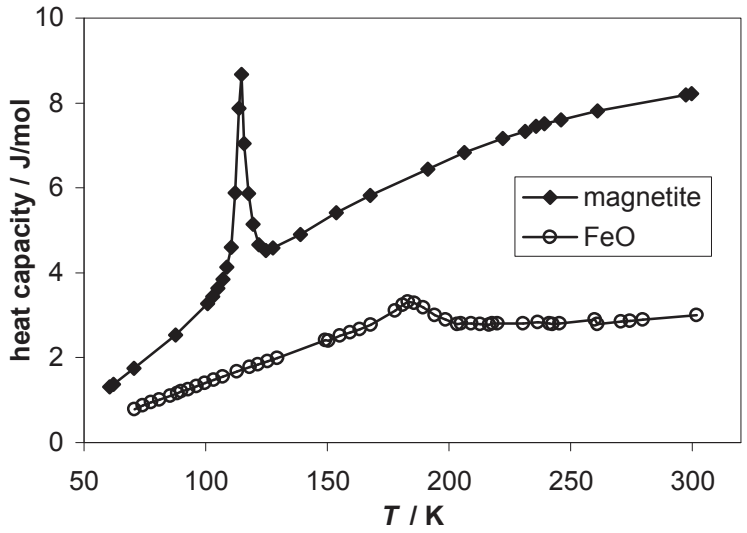

Figure 1.10: One of first specific heat measurements on natural magnetite indicating a phase transition (here at 115 K), together with similar measurements of FeO. Adapted from [47].

1.5.4 Magnetite at high pressures

Besides temperature and magnetic field, pressure is another useful parameter that can be varied to reveal additional properties of magnetite. To induce observable changes, however, quite high pressures are needed.

Remarkably striking conclusions come from the work of Rozenberg et al. [60], where they observed a transition from inverse to normal spinel at pressures 0 to 20 GPa. Other studies [68] have identified a quantum critical point at 8 GPa, where T_V is suppressed to zero.

The question of magnetite properties at high pressures is far from being answered, as there is a number of technical aspects (uniaxial vs hydrostatic pressure, possible sample deformation, etc.) that needs to be thoroughly evaluated and analysed.

1.6 Magnetic measurements

As the main topic of the thesis are magnetic properties of magnetite, it is appropriate to devote a whole chapter to review the existing results of various kinds of magnetic studies.

1.6.1 Susceptibility measurements

Susceptibility measurements were traditionally performed with the sample as the core of a coil or transformer in a bridge arrangement. In more modern measurements the output of the transformer (often in a gradiomemter arrangement) is measured directly by an ac voltmeter or lock-in amplifier (see Section 2.2.2). As the sensitivity of these methods is generally inferior to the SQUID magnetometer and often quite large exciting ac field is necessary, the results will not be reviewed in greater detail. One exception exists where transformer-based methods give additional information - they can overcome the limitations imposed by the demagnetisation effects (see Section 1.1.4). Figure 1.11 is an example of such measurement where a synthetic magnetite single crystal was trimmed to a toroidal shape and used as the core of a transformer. In this case susceptibility

as high as 500 (S.I. units) can be measured, revealing the details of the Verwey transition and the easy axis reorientation. Below the T_V the susceptibility is much lower ($\chi' \approx 1...2$) and it can be measured in a conventional magnetometer. The inset in Figure 1.11 also shows the frequency-dependent glass-like transition (see Section 3.4) and presumably the lowest temperature is low enough that an anomalous transition (see Section 3.5) should be also visible but remains in the non-excited state.

1.6.2 Magnetic after-effect measurement

Magnetic after-effects (also called disaccommodation effects or magnetic viscoelastic effects) are in general spontaneous changes (relaxation) of ac magnetic susceptibility occurring in a magnetically ordered sample after its magnetic domain structure has been severely disturbed, e.g. by strong pulses of applied

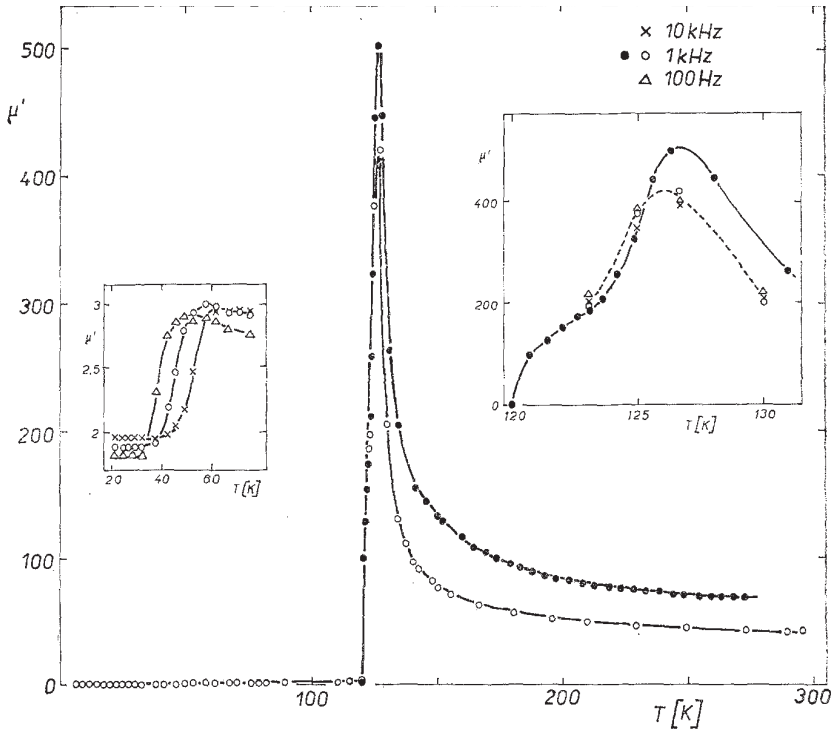

Figure 1.11: Temperature dependence of a stoichiometric magnetite toroidal sample acting as the core of measuring transformer. The demagnetising factor is virtually zero, which allows very high susceptibilities to be measured (such as near the easy axis reorientation temperature at 126 K). The left inset shows the frequency-dependent glass-like transition around 40 K. The right inset shows detail of the Verwey transition and the easy axis reorientation. The filled symbols were acquired in stronger ac field (3.2 A/m) than the open symbols (1 A/m). Adapted from [64].

magnetic field. During this relaxation the domain walls tend to find progressively deeper potential minima (or the potential minima tend to deepen due to e.g. diffusion of impurities towards the domain walls); the ac susceptibility is probed by sufficiently weak ac magnetic field.

There are a number of ways to probe theses relaxation phenomena (see e.g. [15, 31]), however, the most elaborate experimental technique and result presentation and discussion was developed by H. Kronmuller [37] and F. Walz [70]. With this rather unique and time-consuming technique they had studied perhaps all kinds of magnetic materials, paying also attention to magnetite [71–74] and a topical review [75].

The isochronal MAE spectra present the relative change of susceptibility at specific times after a demagnetisation event at given temperature. The demagnetisation event (e.g. a series of strong magnetic pulses) is assumed to be completed at time $t_0 = 0$. The initial susceptibility χ_1 is measured at a certain time t_1, typically 1 second after the demagnetisation. Subsequently another susceptibilities χ_n are recorded at times t_n. Then the quantity $(\chi_1 - \chi_n)/\chi_n$ is plotted for selected times t_n and all temperatures, which results in an isochronal MAE spectrum (see Figure 1.12).

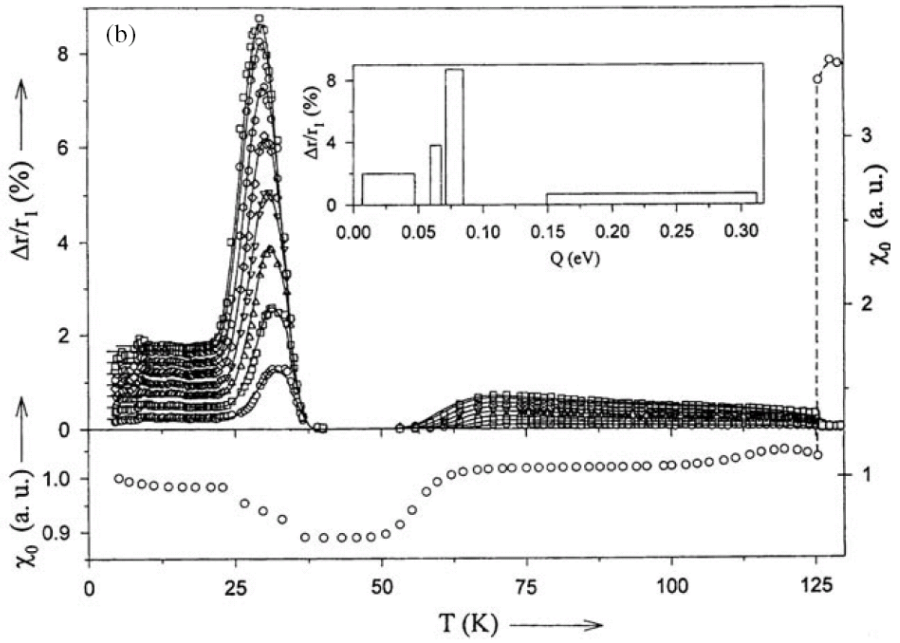

Figure 1.12: An isochronal MAE spectrum of stoichiometric magnetite recorded at times (2, 4, 8, 16, 32, 64, 128, 180) s, together with the initial ac susceptibility at time $t_1 = 1$ s. Adapted from [73].

1.6.3 NMR measurements

NMR is one of methods that can provide detailed microscopic information about magnetite. A remarkable example of such measurement is the work of Novak *et al* [52], that is illustrated in Figure 1.13. The most important conclusions from these data are that the observed line pattern is consistent with a Cc symmetry and that no 'static' charge ordering (on the timescale of the measurement) is observed in magnetite.

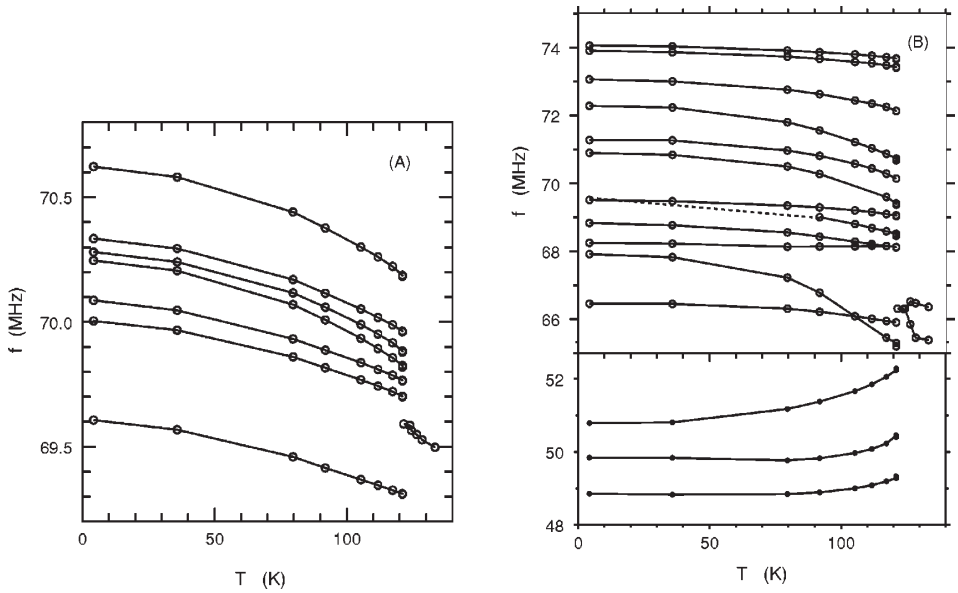

Figure 1.13: Temperature dependence of the NMR frequency of lines corresponding to Fe ions on tetrahedral (A) and octahedral (B) sites. Adapted from [52]. Sample equivalent to B1 measured in zero external magnetic field with a spin-echo method.

2. Materials and Methods

2.1 Samples

2.1.1 Magnetite samples

The samples used through this work were high quality single crystals of magnetite. The samples originate from two sources:

- H samples - grown by the Skull Melter (also called Cold Crucible) method in the laboratory of J. M. Honig
- B samples - grown by the Floating Zone technique by V. A. M. Brabers

For details of these techniques see Section 1.4.2. All the samples were prepared carefully to achieve high homogeneity and desired level of oxygen non-stoichiometry or doping. Most measurements were performed on perfect samples as close to stoichiometry as possible. For a list of magnetite samples and their basic properties see Table 2.1.

Table 2.1: A summary of magnetite samples used through this experimental work together with their basic properties. The non-stoichiometry is expressed as $Fe_{3(1-\delta)}O_4$.

sample	shape	size	δ (10^{-3})	T_V (K)	note
H1	prism	$2.1 \times 2.3 \times 3.1$ mm^3	0	122.2 ± 0.3	
H2	platelet	$8 \times 13 \times 1.8$ mm^3	0	122 ± 0.3	not annealed
B1	cylinder	$h = 4$ mm, $\varnothing = 5$ mm	0	121.5 ± 0.3	
B1-1	disc	$h = 1$ mm, $\varnothing = 5$ mm	0	121.5 ± 0.3	
H3	pyramid	$1.5 \times 1.5 \times 2$ mm^3	2	117.5 ± 0.5	
H4	irregular	mass = 0.66 g	3.5	107.2 ± 0.5	
H5	irregular	mass = 0.31 g	12	100 ± 1	

2.1.2 Other samples

As of yet, it seems that no other samples display features similar to that of magnetite (e.g. something that could be called the Verwey Transition) at similar temperatures. For this we have focused on magnetite.

2.2 Magnetic measurements

There are two basic methods to study magnetic properties of solid. One is based on measuring forces that appear when a sample is placed into appropriate magnetic field. This method allows precise quantitative measurements of even weak

susceptibilities of paramagnets and diamagnets, as well as measurements of spontaneous magnetisation of substances with ordered moments. The other group of methods incorporates electric coils to create (detect) magnetic field (flux). With the introduction of digital signal processors and personal computers the coil-based techniques are easy to implement and yield precise and repeatable results, although to get truly quantitative results an elaborate calibration is essential.

There are numerous other techniques to study magnetic properties of solids, e.g. microwave loss measurements [6], magnetic fluctuations measurements [11], neutron scattering, Hall effect [77], optical methods (based on Kerr effect [14] and Lorentz method [46]), Lorenz transmission electron microscopy, X-ray topography [46] and Bitter technique, to name just a few. However, these techniques were not used extensively during the experimental work related to this thesis and as such will not be described here in any detail.

2.2.1 Force magnetometers

Force measurements have evolved into a very precise and sensitive method allowing, for example, quantification of gravitational forces between objects weighing several kg. A weakly magnetic (para or dia) sample in a homogeneous magnetic field (such as that produced by Helmholz coils) develops homogeneous magnetic moment parallel to the applied field and no force is exerted on the sample. A field gradient is necessary to produce a gradient of the free energy (i.e. force)

$$\frac{\mathbf{F}}{V} = \mathbf{M} \cdot \nabla \, \mathbf{B} \, . \tag{2.1}$$

Thus, in a device called Faraday balance the susceptibility is calculated from

$$\frac{F_x}{V} = \mu_0 \chi H \frac{\partial H}{\partial x} \, . \tag{2.2}$$

A field gradient is not necessary if one is interested in measuring the spontaneous magnetisation of a sample. From the expression for Zeeman energy (energy of a dipole in magnetic field)

$$E = -\mu_0 \, \mathbf{m} \cdot \mathbf{H} \tag{2.3}$$

it follows that a torque is exerted on a magnetic moment (or magnetised sample) in homogeneous magnetic field

$$\frac{\tau}{V} = \mu_0 \, \mathbf{M} \times \mathbf{H} \, . \tag{2.4}$$

These methods allows precise quantitative measurements of static properties (spontaneous magnetisation, static magnetic susceptibility, anisotropy), but due to the long time constant of high-precision force measurements, they cannot be used for ac susceptibility measurements or fast relaxation measurements.

2.2.2 Induction magnetometers

Generally, induction magnetometers rely on electrical coils when generating and sensing magnetic field. There are many variations on this theme:

- ac susceptometer - the sample acts as a core of a transformer with two copper windings: one generates the applied (ac and dc) magnetic field and the other senses the ac response of the sample. Due to the laws of induction the sensitivity drops linearly with decreasing frequency, so the susceptometer usually operates at frequencies above 100 Hz.

- vibrating sample magnetometer - the sample moves periodically in the sensing coil, so the spontaneous dc magnetic moment can be measured. When equipped with the field-generating coil, the $M(H)$ dependence can be measured. The same principle may be used in a slightly different arrangement - the vibrating coil magnetometer.

- SQUID magnetometer - instead of ordinary Cu coils the instruments above can be equipped with a SQUID (See Section 2.2.3). Apart from enhanced sensitivity the SQUID allows measuring at very low frequencies (down to zero), and thus can measure both ac properties and spontaneous magnetization conveniently.

Often the sensing coil is used in a *gradiometer* arrangement - two coils in series with opposite winding directions. Such system of coils is insensitive to the homogeneous driving field and only senses the magnetic response of the sample centred in one of the coils. With a gradiometer much higher sensitivity can be achieved and weakly paramagnetic and diamagnetic samples can be measured reliably.

Depending on the versatility of field generation and the processing of sensed signals there is a large number of possible measuring methods, such as magnetic noise measurements (with no applied field the fluctuations of magnetisation is related to the imaginary part of ac susceptibility [11]) or relaxation phenomena (also called disaccomodation or *magnetic after-effects* - MAE [31], see Section 1.6.2).

2.2.3 SQUID magnetometer

One of the most striking properties of superconductors - the existence of macroscopic wavefunction $\psi = \sqrt{n_s}\mathrm{e}^{i\varphi}$ as postulated by Ginzburg and Landau [20] - leads among others to quantisation of magnetic flux through a continuous superconducting loop. As the change of the phase of the wavefunction φ is intimately related to the magnetic flux Φ enclosed in a superconducting loop by

$$\Delta\varphi = \frac{e\Phi}{\hbar} \,, \tag{2.5}$$

and realising that single-valued phase is ensured by quantisation condition $\Delta\varphi = 2\pi n$, we arrive at the quantisation of magnetic flux in a continuous superconducting loop

$$\Phi = n\Phi_0 \,,\ \Phi_0 = \frac{h}{2e} = 2.07 \cdot 10^{-15}\ \mathrm{Wb} \,. \tag{2.6}$$

One particularly important implication of this quantisation is that the flux inside a superconducting loop is always conserved unless a quantum Φ_0 is forced to pass the wire - this is exploited e.g. in a superconducting transformer (see later in this chapter).

The superconducting loop can be interrupted by one or two "weak links" - so called Josephson Junctions. The interference of the macroscopic wavefunctions at opposite sides of the junction can lead to peculiar effects - so called dc and ac Josephson effects [26, 27]:

- the dc Josephson effect
$$j = j_c \sin \Delta\varphi \tag{2.7}$$
describes the dependence of a dc superconducting current j on the difference of phases of the wavefunctions $\Delta\varphi$ at both sides of the junction; the critical current j_c depends on the material, the junction geometry and temperature.

- ac Josephson effect
$$\frac{\partial}{\partial t}\Delta\varphi = \frac{2e}{\hbar}V \tag{2.8}$$
prescribes the relation between the time evolution of the phase difference $\Delta\varphi$ and the voltage V across the junction; the junction is no longer in superconducting state and energy is dissipated.

On the basis of these two Josephson effects a superconducting quantum interference device (SQUID) can be constructed. A dc SQUID is a superconducting loop interrupted by two Josephson junctions. The critical superconducting current passing through the SQUID is a periodic function of the enclosed flux Φ with a period of Φ_0. Similarly, an ac SQUID is a superconducting loop interrupted by a single Josephson junction. Then the energy dissipated by the ac SQUID (when driven with weak ac field at several MHz) is again a periodic function of the enclosed flux Φ with a period of Φ_0. To construct a magnetometer with such sensitive and nonlinear device a feedback loop is constructed that keeps the flux through the SQUID at a constant level by means of an additional feedback coil (see Figure 2.1). The feedback loop is locked to one of the extrema of the periodic

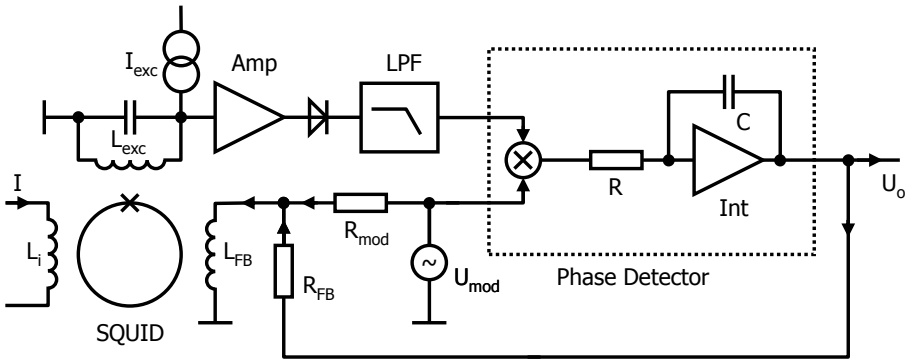

Figure 2.1: A simplified schematic of an ac SQUID magnetometer. L_i - input coil (a part of the superconducting gradiometer), L_{exc} - excitation coil, I_{exc} - excitation current ($f_{exc} \approx 30$ MHz), Amp - radio-frequency amplifier, LPF - low pass filter ($f_T \approx 1$ MHz), Int - integrator ($1/RC \approx 1$ kHz), L_{fb} - feedback coil, U_{mod} - modulation source ($f_{mod} \approx 100$ kHz). U_o is the output voltage proportional to the input current, $U_o(t) = A \cdot (I(t) - I(0))$, where A is the gain of the feedback loop and $I(0)$ is the input current at the moment the feedback loop was locked.

SQUID response. To maintain the operating point of the SQUID in the vicinity of given extreme a weak modulation current (at several kHz) is added to the feedback coil and the symmetry of the SQUID response is detected by a phase detector that locks the feedback loop. With a careful design a spectral noise density of $10^{-4}\Phi_0 \mathrm{Hz}^{-1/2}$ can be achieved allowing exceptionally high sensitivity of the method.

A schematic view of a practical SQUID magnetometer is presented in Figure 2.2. A superconducting solenoid operating in non-persistent mode is capable of generating ac and dc magnetic fields up to 25 mT. The sample response is sensed by a superconducting gradiometer which forms the primary of the superconducting transformer; the secondary is coupled to the SQUID itself (See Figure 2.1). The sample is attached to a sapphire holder that stabilises the sam-

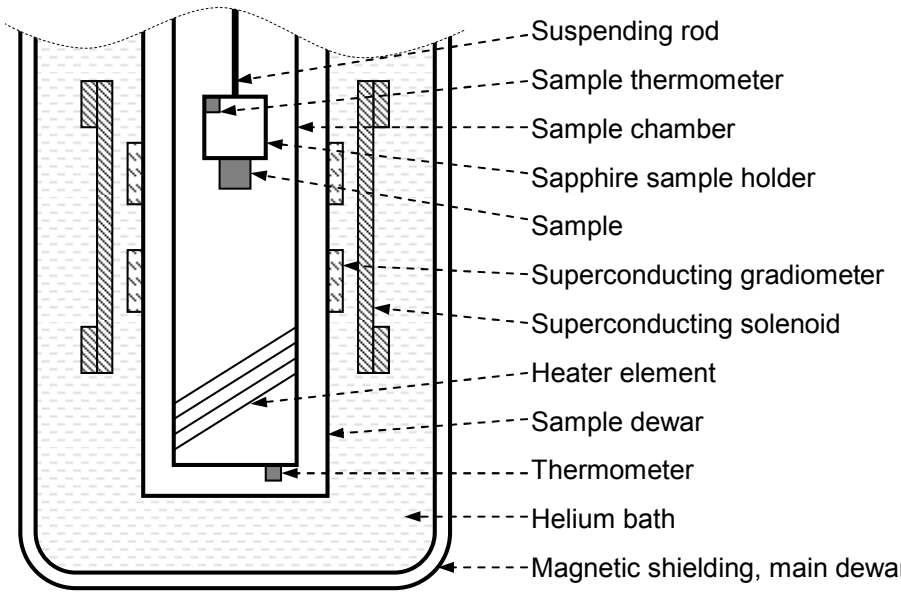

Figure 2.2: A simplified schematic of a practical SQUID magnetometer.

ple temperature and provides good thermal contact to the sample thermometer. The thermal contact between the sample holder and the walls of the anticryostat (the sample chamber) is provided by He gas at atmospheric pressure. The anticryostat temperature is controlled by a resistive heater and an additional thermometer (see Section 2.4. Technical details can be found in [24].

It is worth noting than MAE spectroscopic measurements (as described in Section 1.6.2) can be in principle conducted on our SQUID magnetometers, provided a sufficiently strong magnetic field can be generated to demagnetise the sample. It has to be noted, however, that due to the optimisation of the SQUID system to low frequency measurements (several Hz instead of kHz), these measurements tend to be even more time-consuming, with subsequent difficulties with liquid He refilling during experiment.

2.3 Electric transport measurements

2.3.1 Dc conductivity measurements

There are two main approaches to electrical resistance measurements: either one can measure the voltage drop when a constant current is made to flow through the sample or a constant voltage is applied and the current is measured. Either way, the resistance is calculated from the simple formula

$$R = \frac{U}{I} \,. \tag{2.9}$$

The resistance then may be expressed in terms of intrinsic material properties (conductivity or resistivity) by scaling with a geometrical factor, that can be calculated analytically for simple sample geometries.

Electrical conductivity of magnetite varies over many orders of magnitude with temperature. In the high conductivity range (for resistances below 10 kΩ) the voltage drop on the connecting leads may affect the precision of the results, so a four-probe technique is used, where both current source and voltage sensing circuit use dedicated pairs of wire. These measurements were performed with a HP Agilent 34401A precision multimeter equipped with resistance ranges from 100 Ω up to 10 MΩ with a constant current ranges of 1 mA to 0.5 μA (making up to 5 V input compliance, 1 V at low-resistance ranges). Due to the switching of current ranges throughout the measurement the resulting applied voltage changes abruptly and the dissipated power is a non-trivial function of resistance (being highest - 1 mW - at 1 kΩ and around 2.5 μW at the highest resistance - 10 MΩ).

When measuring very high resistances (megaohms, gigaohms) the four-probe technique is unnecessary; much more attention must be devoted to minimising any leakage current due to connecting leads. High resistance measurements were performed with a Keithley 6517A electrometer, generating constant voltage (as high as 400 V) and sensing the current flow through the sample allowing values as high as 100 TΩ to be measured. Due to the higher voltage the power dissipation is also higher, but it is less than 1 μW within the gigaohm ranges.

2.3.2 Ac dielectric measurements

Generally, when a harmonic ac current $I(t) = I_1 \cos(\omega t)$ is made to flow through an impedance Z the voltage developed across the sample $U(t)$ may be phase-shifted, that is $U(t) = U_1 \cos(\omega t + \varphi)$. Then a complex impedance Z is defined as

$$Z(\omega) = \frac{U_1}{I_1} \mathrm{e}^{i\varphi} \,, \tag{2.10}$$

and it can easily be measured with a lock-in amplifier that reports both the in-phase and the $\pi/2$ delayed component of the voltage $U(t)$. The complex impedance Z can also be expressed in other forms, e.g. as a parallel or serial R-C combination, etc. All these forms are equivalent and are mutually connected with simple formulas in which only the frequency ω appears.

Dielectric (or complex-impedance) properties were probed with a HP Agilent 4284A precision RLC meter, capable of operating in frequency range from 20 Hz to 1 MHz with a PLL-controlled current source capable of delivering from 50 μA

to 20 mA, the measured voltage ranges are from 5 mV to 2 V. It offers a four-probe measurement (four coaxial shielded cables) with a special compensation scheme to minimize the effects of voltage drops and capacitances of the cables. The reliability of the results strongly depends on the frequency, the cable length and the properties of the sample.

Another source of possible errors, that needs great attention, is the electrical connection of the sample itself. Either the electrical bonds may be unstable and the measured resistance change unpredictably with temperature, or a charged insulating layer may form at the metal-sample interface, leading to effects such as Maxwell-Wagner relaxation [41].

2.4 Temperature measurement and control

The ability to control the sample temperature with high precision and stability is a necessary condition for studying sharp transitions, such as the onset of superconductivity and the Verwey transition. Our temperature control system consists of a resistive heater, two temperature sensors (GaAs or Si diodes) and a PID controller.

As can be see from Figure 2.2 the studied sample and the sample temperature sensor are only loosely thermally coupled to the heater element. Due to this weak thermal coupling a PID loop closed between the heater and the sample thermometer would suffer from unacceptably slow response and would be prone to oscillations. To solve this problem an additional thermometer was anchored to the inner surface of the anti-cryostat, in good thermal contact with the heater. The PID loop between the heater and this auxiliary thermometer has faster response (several seconds) and allows for precise regulation of the anti-cryostat temperature. The sample temperature is slightly higher (by about 0.5 K) due to the heat input through the suspending rod. This difference is, however, fairly constant in the steady state and does not affect the sample temperature stability.

Together with the associated PID controller the achieved temperature resolution is 0.1 mK, short-term stability is 1 mK, repeatability is about 10 mK and the absolute accuracy is better than 0.5 K (when the temperature is ramped reasonably slowly and in the absence of latent heat produced or absorbed by the sample). The controller conveniently allows linear ramping of the setpoint temperature with a rate of 10 K/min down to 0.001 K/min.

A modified sample holder was designed and used for semi-quantitative latent heat measurements. In this case the desirable weak thermal coupling between the sample and the surrounding anti-cryostat was achieved by evacuating the sample chamber (down to $\approx$ 30 Pa) and suspending the sample on thin nylon fibres. The sample temperature was monitored by a resistive thermometer (Cernox) glued directly onto the sample. The difference of the sample and the chamber temperatures was used as a measure of heat transfer and together with a simple model the ratio of the latent heat to the specific heat could be obtained with good precision (see the results in Section 3.3.1).

3. Results on stoichiometric magnetite

3.1 Samples overview

The samples used throughout this work are summarized in Section 2.1. Due to the necessary high quality of samples and the difficulties preparing them, only two sources of synthetic magnetite are used - the samples denoted H originate from the laboratory of J. M. Honig and the samples denoted B came from V. A. M. Brabbers. In this chapter the results obtained with stoichiometric samples are presented. As explained in the Section 1.4.1, no natural samples were measured.

3.2 Overall ac susceptibility

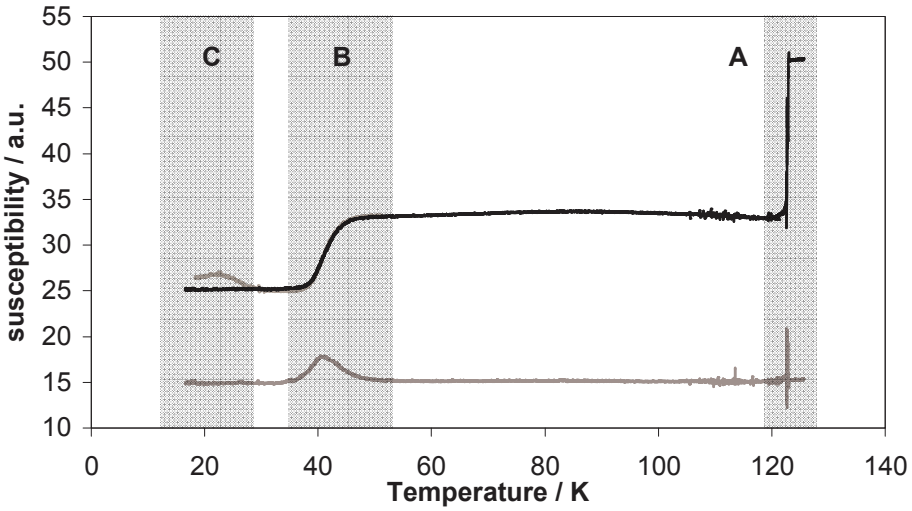

Figure 3.1: An overview of the temperature dependence of ac complex susceptibility of a typical high-quality stoichiometric magnetite sample. Three regions of interest are highlighed: A - the Verwey transition, B - a frequency dependent feature called glass-like transition, C - a low temperature anomaly, where under certain conditions the susceptibility may attain higher value than the baseline. Sample H1, $\mu_0 H_{ac} = 10$ μT, $H_{dc} = 0$, cooling rate 2 K/min.

Figure 3.1 depicts a typical temperature dependence of ac complex susceptibility of stoichiometric magnetite. Because in weak fields there are not many features visible on the $\chi(T)$ dependence and due to the long measurement time required to acquire such data we focused on three main temperature regions, as depicted in the figure. These are:

A - The Verwey transition, the most prominent feature in magnetite below room temperature, will be further studied in Section 3.3.

B - So called glass-like transition, a frequency dependent feature at lower temperatures (around 40 K), is presented in Section 3.4.

C - A new relaxation phenomenon, the low-temperature anomaly taking place below 30 K, will be further described in Section 3.5.

An individual chapter is devoted to each of these transitions, presenting results of both magnetic (mainly ac complex susceptibility, spontaneous magnetisation) and dielectric measurements (dc resistivity, ac complex permittivity) at various conditions.

3.3 The Verwey transition

Although the Verwey transition is the most important phase transition in magnetite below room temperature, accompanied by changes of electric conductivity, magnetocrystalline anisotropy and lattice symmetry, its study on our SQUID magnetometer is limited. This is due to the fact, that the observed $\chi(T)$ does not depend on the frequency and magnitude of the applied magnetic fields in the ranges accessible with our equipment. Some important results pertaining the Verwey transition are detailed below.

3.3.1 Latent heat of the phase transition

Although the aparatus (see Section 2.2.3) is not specifically designed to measure specific or latent heat of a sample, by simply thermally insulating the sample and attaching a thermometer directly on the sample surface the latent heat of transition, i.e. the region where the sample temperature is held constant by the evolution or absorption of the latent heat, can clearly be identified, see Figure 3.2. This is clear manifestation of first order phase transition, as is expected for stoichiometric magnetite. Another important feature seen from the figure is the random variation of the spontaneous magnetization M during the phase transition.

The measurement is, however, only qualitative, as the absolute amount of heat flowing into the sample through a simple insulation (suspension on a pair of nylon fibres, He gas evacuated to 30 Pa) during uniform warming could not be reliably estimated. A rough estimate of the latent heat can be given based on fitting a simple model, that accounts for various heat-leakage paths and temperature sensor offset. Based on the known values of specific heat of synthetic magnetite at 120 K, $c_p = 75\ \mathrm{J\,mol^{-1}\,K^{-1}}$ [16], a value of latent heat $L = 0.63 \pm 0.1\ \mathrm{kJ\,mol^{-1}}$ can be estimated (see Figure 3.3). This value compares surprisingly well with the values found in [34], where the entalphy of the Verwey transition is reported in the range from 0.6 to 0.7 $\mathrm{kJ\ mol^{-1}}$ for stoichiometric and nearly stoichiometric magnetite.

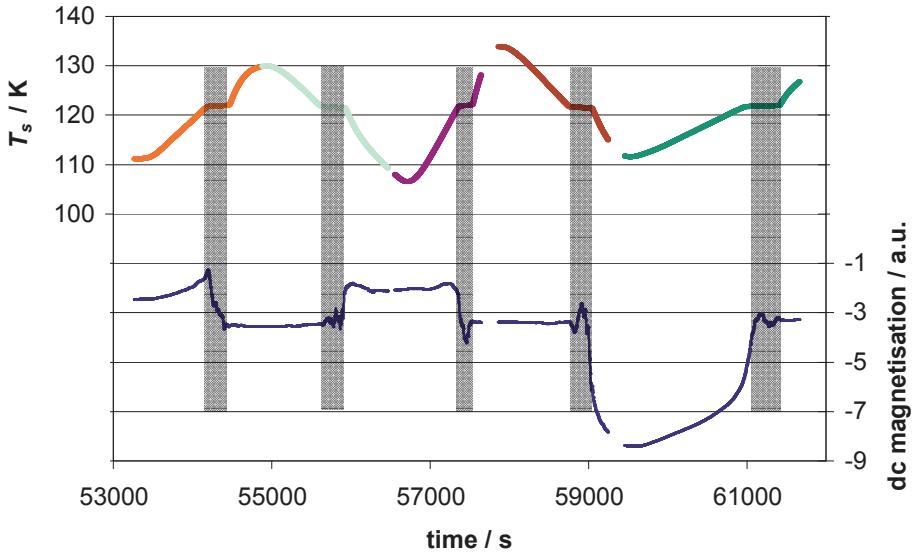

Figure 3.2: Measurement of sample temperature T_s and spontaneous magnetization during cycling through T_V. The regions of the phase transition are highlighted in grey. Visible is the first-order character of the phase transition and random variations of spontaneous magnetization during the transition. Sample H2, $H_{ac} = 0$, $H_{dc} = 0$, sample chamber He gas pressure 30 Pa.

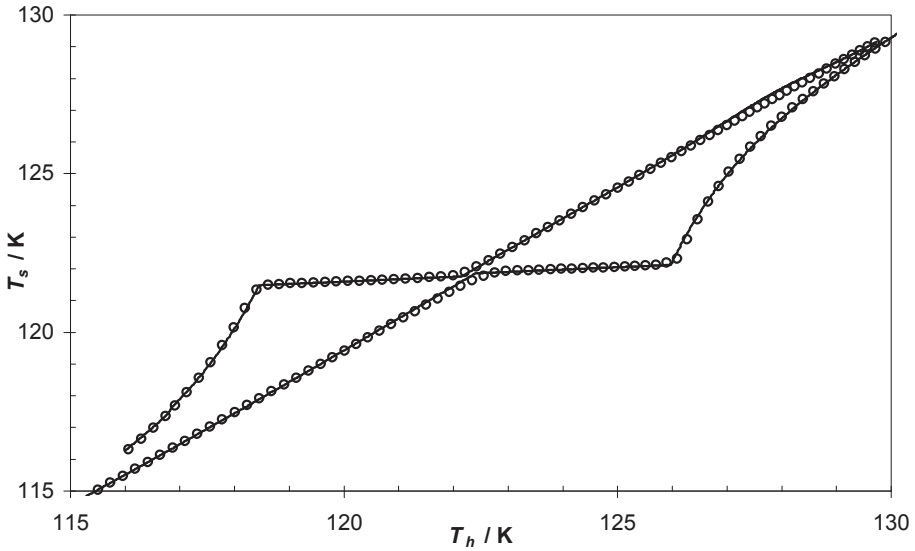

Figure 3.3: The sample temperature vs the holder temperature, during cooling and warming 5 K/min. The model (solid line) corresponds well to the experimental points (circles). The model assumes thermal coupling of the sample to the sample holder and to the anti-cryostat walls. Other free parameters are the latent heat and the sample sensor offset. Sample H2, $H_{ac} = 0$, $H_{dc} = 0$, sample chamber pressure 30 Pa.

3.3.2 Thermal hysteresis in magnetic measurements

Among all the features and transitions found in magnetite below room temperature only the Verwey transition, as a first order phase transition, may exhibit some hysteresis with respect to temperature, as exemplified by Figure 3.3. This

is further illustrated in Figure 3.4, where an attempt was made to stabilize the temperature in the middle of the transition. The resulting $\chi'_{ac}(T)$ dependence

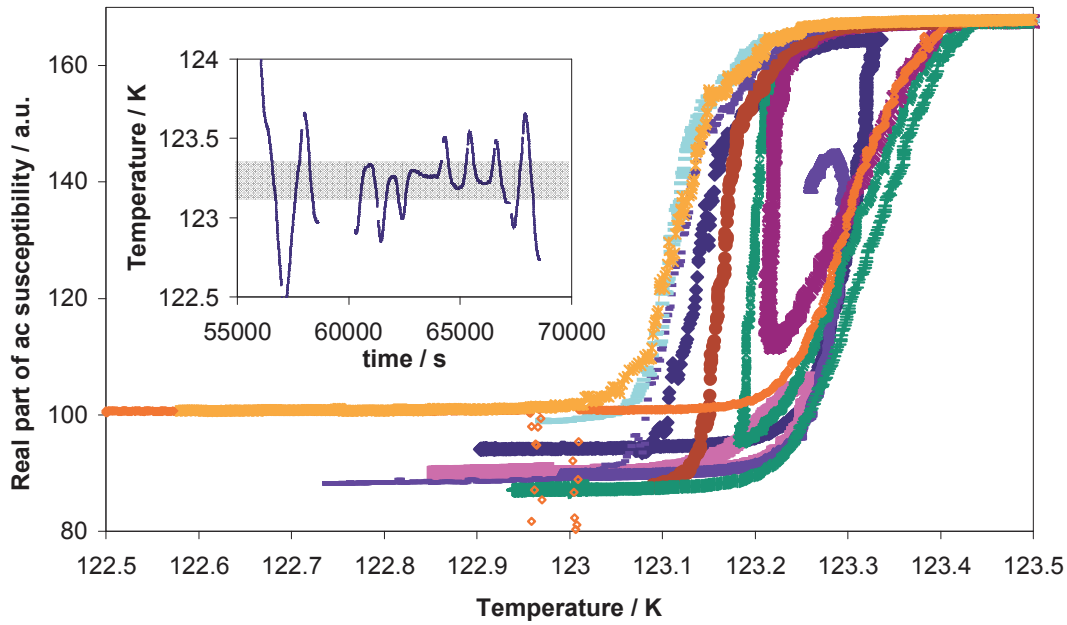

Figure 3.4: The detailed $\chi'(T)$ measurement during traversing the Verwey transition. Illustrated is the hysteresis of the transition and the fact that the magnitude of the susceptibility below T_V is unique for each run. The measured susceptibility above T_V is limited by the demagnetising effect. The inset shows the time course of the experiment (overall duration nearly four hours). Sample H1, $\mu_0 H_{ac} = 10$ μT, $H_{dc} = 0$.

shows this hysteretic behaviour and it is apparent, that the coincidence of $\chi'_{ac}(T)$ curves on cooling and warming cannot be achieved even in the limiting case of extremely slow warming/cooling.

The same behaviour under controlled warming/cooling rates is depicted in Figure 3.5. Obviously, high rates of temperature change lead to wider hysteresis

than low rates. However, extrapolation to a rate of 0 K/min leads to a hysteresis of T_V of about 0.3 K.

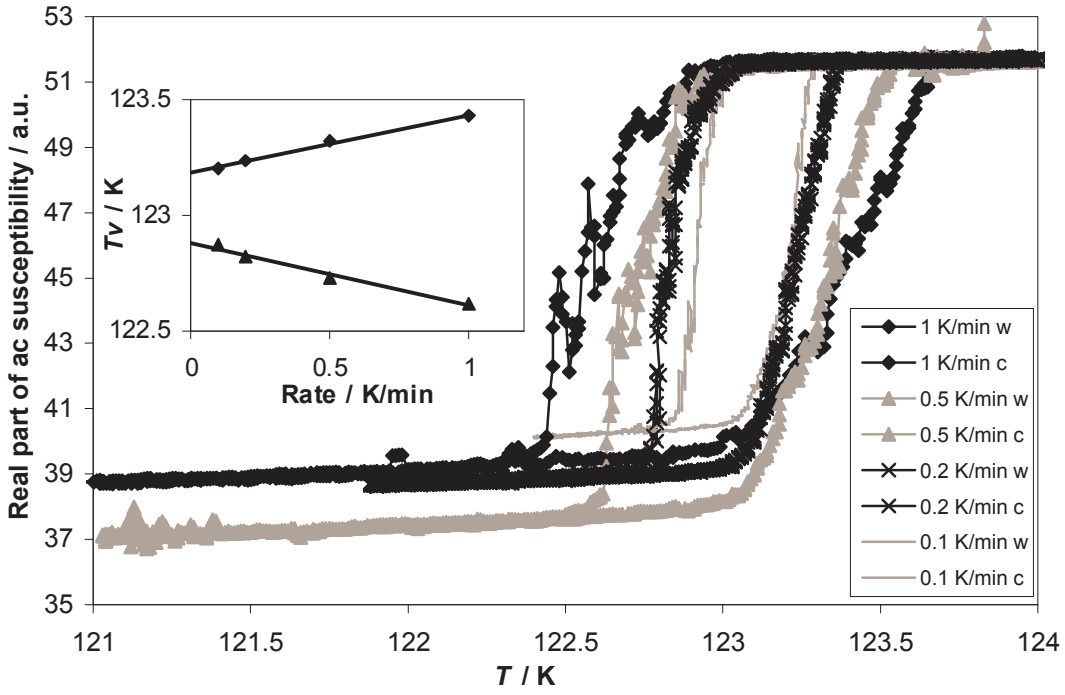

Figure 3.5: Detail of the thermal hysteresis of the Verwey transition in weak field for cooling and warming rates of 1.0, 0.5, 0.2, 0.1 K/min. The inset shows the dependence of the transition temperature on the rate of cooling/warming. Sample H1, $\mu_0 H_{ac} = 1$ μT, $H_{dc} = 0$.

3.3.3 Behaviour of spontaneous magnetization

As was already mentioned in Section 3.3.1 and especially in Figure 3.2, even in the absence of any applied magnetic field the spontaneous magnetization M of the sample varies randomly and unpredictably. Not only the magnitude of the change of M is random, even the sign of its change varies with each cycle through T_V. It is well known that the saturated magnetisation M_s does not change appreciably at the Verwey transition (see Figure 1.7), thus these fluctuations may only be caused by a random rearrangement of magnetic domains. It appears that below T_V the absolute value of sample magnetization is more variable than above, i.e. the magnetisation after warming through the transition often stabilises at the same value.

If a strong dc magnetic field is applied when the sample is cooled and warmed through T_V, the random fluctuations are suppressed by the large $M(T)$ sample response when passing the transition, see Figure 3.6. Even in a moderate field of

± 2 mT the sample response exceeds the range of the SQUID by a factor of five and the data processing (stitching) may introduce errors into the $M(T)$ dependence. Additionally, the impact of nonzero demagnetising factor cannot be neglected.

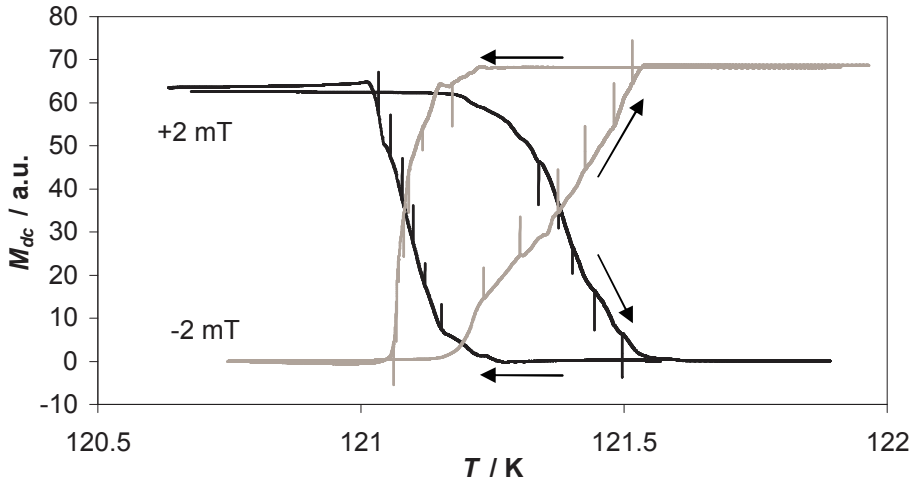

Figure 3.6: The temperature dependence of magnetisation of magnetite sample when cooled and warmed through T_V in a dc magnetic field. The vertical bars represent events when the SQUID electronics ran out of range ± 10 V and was reset back to 0. This happened several times due to the strong magnetic response of the sample. Sample B1, $H_{ac} = 0$, $\mu_0 H_{dc} = \pm 2$ mT.

3.3.4 Electrical conductivity

To facilitate electrical measurements a suitable disk-shaped sample (thickness 1 mm, diameter 5 mm) was equipped with silver electrodes on opposite sides (diameter 4 mm, magnetron sputtering). The ten orders of magnitude change of dc conductivity below T_V is plotted in Figure 3.7. The high dynamic range

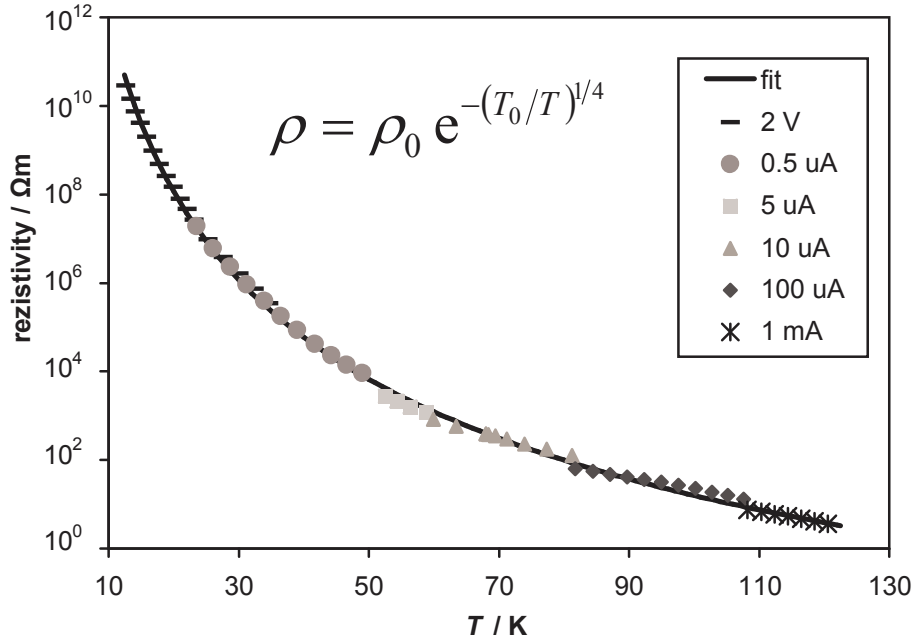

Figure 3.7: Temperature dependence of electrical resistivity below T_V, together with an exponential fit. The legend denotes specific measurement conditions: constant voltage (2 V) or constant current (0.5 μA, 5 μA, 10 μA, 100 μA, 1 mA). Sample B1-1 with magnetron-sputtered silver contacts.

of this measurement is crucial in determining the temperature exponent (about 0.22 ± 0.04 in our measurement, in agreement with Mott's model of Variable Range Hopping, exponent 1/4). If a smaller range is used for fitting, almost any reasonable temperature exponent fits the data satisfactorily.

The discontinuities appearing simultaneously with the changes of measuring ranges (and thus measuring conditions) suggest weakly non-linear behaviour of the sample, i.e. the resistivity decreases with increasing applied voltage. A minor part of this effect may be caused by Joule heat. The nonlinear voltage-current characteristics of the sample was also measured at various temperatures and three such characteristics are depicted in Figure 3.8. The time span of a single period of

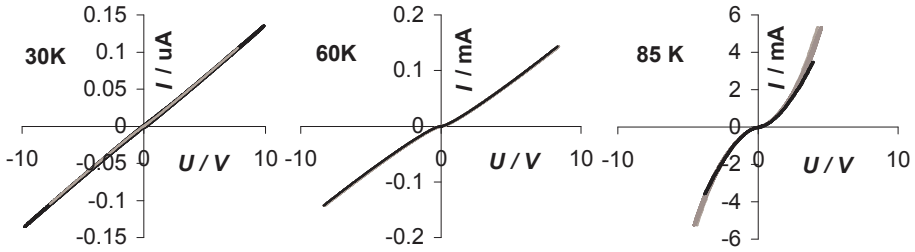

Figure 3.8: Voltage-current characteristics at three temperatures (30K, 60K and 85K) of a magnetite sample. The measuring period was varied from 240 s to 2 ms to ensure that thermal effects are negligible. The Ag electrodes were sputtered on the opposite sides of the B1-1 disc sample.

measurement (triangular bipolar waveform) was varied from 240 seconds to 2 ms to reveal the effects of sample warming and thermal hysteresis. The effect of Joule heating may be discernible above T_V, where the current necessary to maintain a potential difference of the order of 10 V is substantial. At lower temperatures this effect is negligible. The long-period measurements were performed directly with A-D and D-A converters driven by a computer. The short-period measurements were performed with a waveform generator (Agilent 33220A) and digitised with a digital oscilloscope (Tektronix TDS2024C). The current was measured as a voltage drop on a suitably choosen series resistor (100 Ω to 10 MΩ). The nonlinear behaviour was observed in the temperature range from 60 K to 250 K, the feature is most prominent from 90 K to 140 K where the small-signal (100 mV) conductivity was more than order of magnitude lower than the differential conductivity at 5 V.

Based on the nonlinearities of $I(U)$ dependences one may generally expect that the complex susceptibility depends on the amplitude of the applied voltage. To study these effects in greater detail a measurement of higher harmonics of the ac susceptibility would be advantageous. However, it possesses many technical challenges to design such experiment with the frequency spanning several decades.

The Verwey transition itself is accompanied by a sharp change in electrical conductivity. This is illustrated in Figure 3.9, where the sharp increase of

electrical resistivity upon cooling through the Verwey transition, two orders in magnitude, is indicative of high quality magnetite sample.

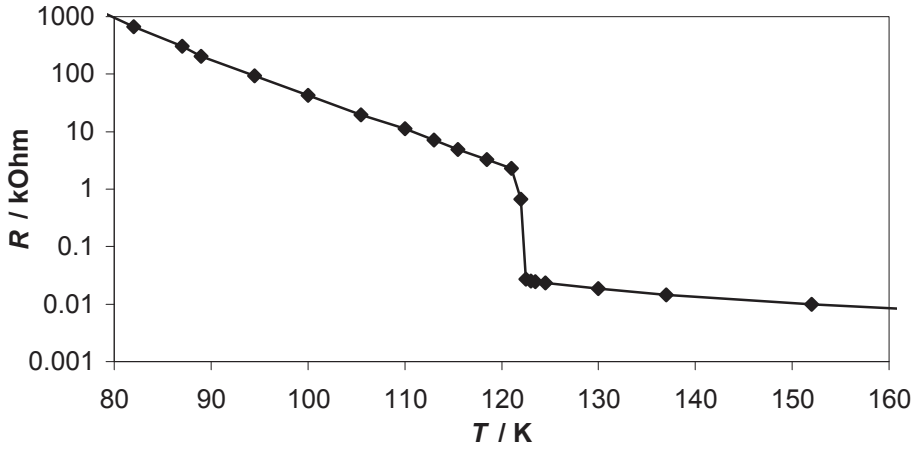

Figure 3.9: Temperature dependence of electrical resistivity around T_V, showing a two orders of magnitude increase of resistivity when cooled through the transition. Sample H2 with ultrasonically bonded gold wire contacts.

3.4 Glass-like transition

So called glass-like transition is a magnetic relaxation phenomenon occurring at 30 − 50 K which can be accurately described by Debye relaxation (see Section 1.1.5) with temperature activation of time constant. As such it displays strong dependence of $\chi(T)$ on frequency of probing magnetic field and is insensitive to the applied field amplitude or dc magnetic field [25]. The results of magnetic and dielectric measurements at low temperatures are summarized below.

3.4.1 Magnetic ac susceptibility

The glass-like transition manifests itself as a gradual increase of real part of ac magnetic susceptibility $\chi'(T)$ with increasing temperature accompanied by a broad dissipation peak (the $\chi''(T)$ dependence). The frequency dependence of this transition is illustrated in Figure 3.10. No temperature hysteresis was observed, the $\chi(T)$ for warming and cooling are indiscernible when a rate of 1 K/min is used.

The shapes of the $\chi'(T)$ and $\chi''(T)$ curves corresponds well to the Debye's model (Section 1.1.5), if Arrhenius temperature activation is assumed to link the Debye's relaxation time with temperature, i.e. $\tau = \tau_0 \exp(E_a/k_B T)$, where E_a is the activation energy and τ_0 is a parameter corresponding to the relaxation time at infinite temperature. However, the temperature exponent (equal to -1 in the Arrhenius' model, $-1/4$ in Mott's VRH model) cannot be reliably determined from the experimental data due to the small relative range of the measurements (less than two orders of magnitude).

Figure 3.11 contains the experimental frequency dependencies of the glass-like transition temperatures $T_g(f)$ for several stoichiometric magnetite samples, together with exponential (Arrhenius) fits. It is apparent that T_g's vary widely among samples, despite the fact, that T_v's of these samples are nearly identical (see Table 2.1). Another remarkable point is the difference between B1 and

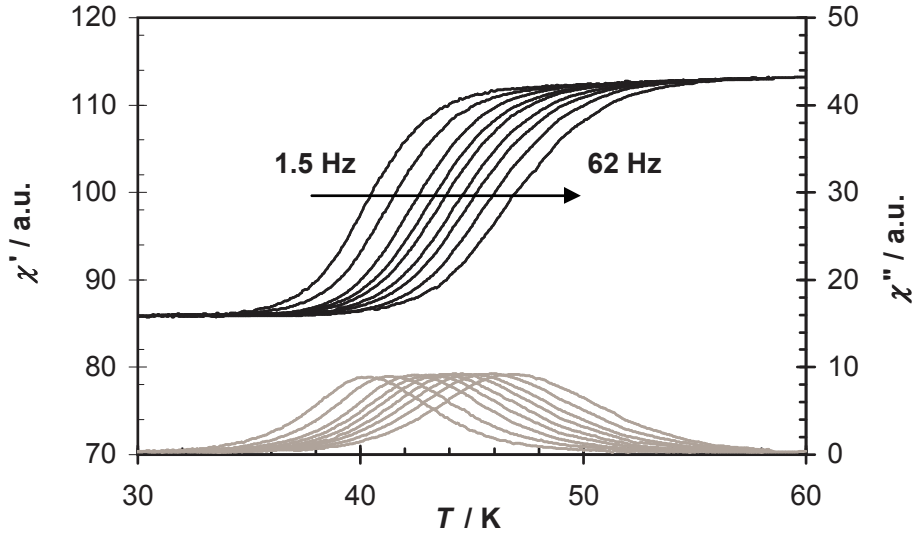

Figure 3.10: Temperature dependence of real part (black lines, left axis) and imaginary part (gray lines, right axis) of ac magnetic susceptibility for frequencies $f = 1.5, 3.1, 6.3, 9.4, 12.5, 18.8, 25, 37.5, 62.5$ Hz. Sample H1, $\mu_0 H_{ac} = 5$ μT, $H_{dc} = 0$.

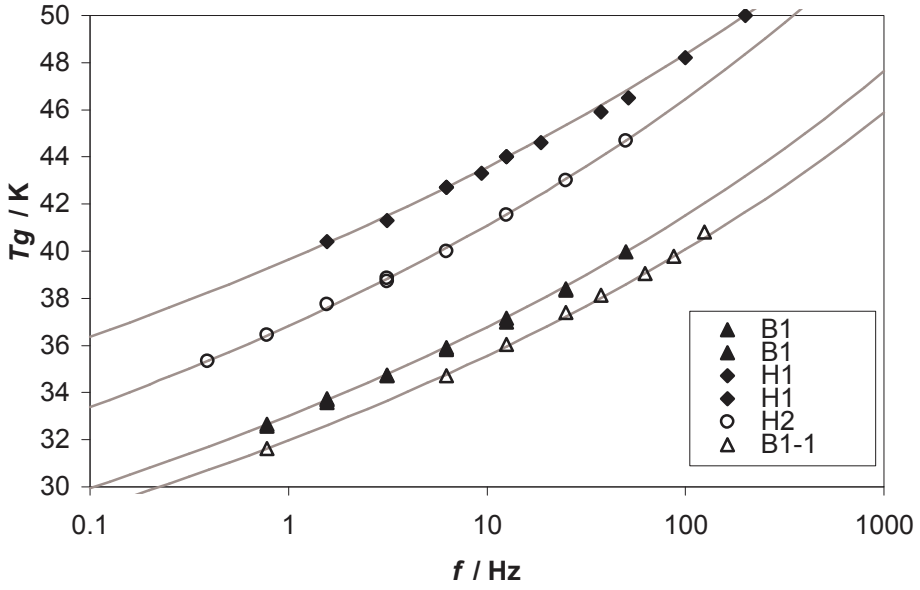

Figure 3.11: A compilation of the transition temperatures of the glass-like transitions T_g versus frequency for various stoichiometric magnetite samples. The points are experimental data (points of inflexion on the $\chi'(T)$ curves), the lines are exponential Arrhenius fits, apparently describing the data quite well. $H_{dc} = 0$.

B1-1 samples, B1-1 being a disk cut out of the B1 sample, so the difference is mainly caused by different demagnetising factor, as discussed in Section 1.1.4 (B1-1 has significantly higher demagnetising factor than B1, leading to lower apparent transition temperature at given frequency). The extracted temperature activation parameters - the activation energy E_a and the time constant τ_0 are summarised in Table 3.1.

Table 3.1: A summary of activation parameters associated with the glass-like transition in stoichiometric magnetite samples. The parameter τ of the measured Debye-like relaxation of complex ac susceptibility is approximated by an exponential Arrhenius temperature-activated process, i.e. $\tau(T) = \tau_0 \exp(E_a/k_B T)$, here E_a is and activation energy and τ_0 is a time constant (attempt period).

sample	E_a / meV	τ_0 / ns
H1	87	0.0079
H2	71	0.22
B1	64	0.17
B1-1	63	0.13

3.4.2 Correlation with dielectric properties

To find whether there is a correlation between magnetic and electrical properties of magnetite at lower temperatures (below T_V) a dielectric spectroscopy was performed on two samples (H2 with ultrasonically bonded gold wire contacts, and B1-1 with magnetron-sputtered silver contacts). Due to more suitable geometry of the sputtered contacts, the experimental results of B1-1 sample will be presented.

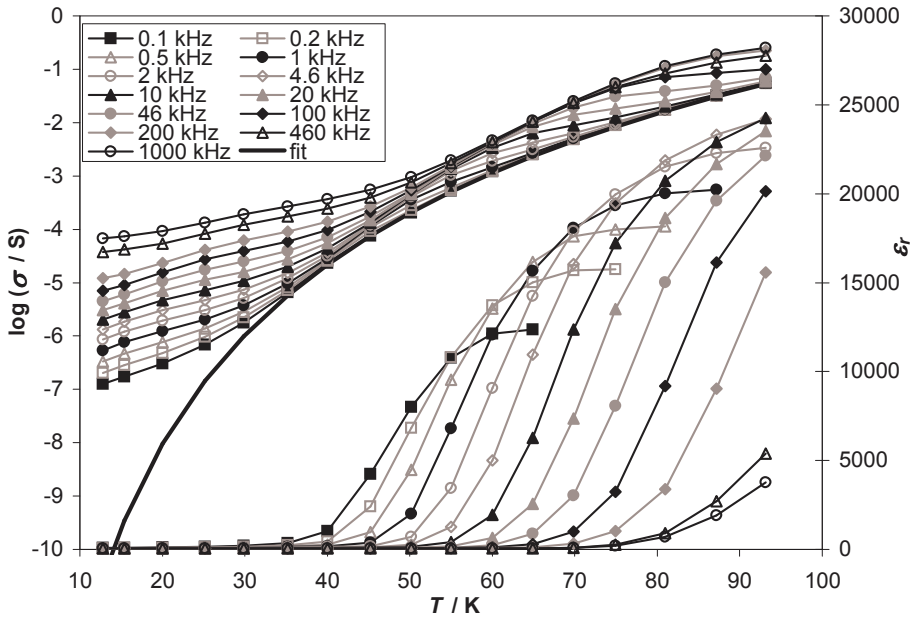

Figure 3.12: Dielectric spectroscopy (impedance) measurement for frequencies 100 Hz to 1 MHz. The complex impedance is expressed as a parallel RC combination, the R and C are then converted to σ (left logarithmic axis) and ε_r (right axis) using simple geometrical model of isotropic dielectric with homogeneous current distribution. The solid line is a fit of the zero-frequency limit of the conductivity according to the Mott's VRH model. Sample B1-1, $U_{ac} = 1$ V, $H_{dc} = 0$.

When the complex impedance Z of the sample is expressed as a parallel RC combination (ideal resistor and ideal capacitor), then the temperature dependence of dielectric properties can be presented as in Figure 3.12. Remarkable is

the extremely high relative permittivity at some frequencies and temperatures, reaching as high as $2.5 \cdot 10^4$, which is typical for some ferroelectric materials near the ferroelectric transition and inhomogeneous samples composed of small insulated conductive grains.

The ac electric conductivity is higher than the dc limit, and the dc limit can be accurately described by Mott's Variable Range Hopping (VRH) model, as discussed in Section 3.3.4. The departure of ac conductivity from the dc limit, that is apparent at temperatures below 30 K, can be described by a frequency dependent conductivity as

$$\sigma(\omega, T) = a(T) \cdot \omega^s \ . \tag{3.1}$$

This approximation is, however, valid only for temperatures below 35 K, as can be seen from Figure 3.13. Here the same experimental data as in Figure 3.12

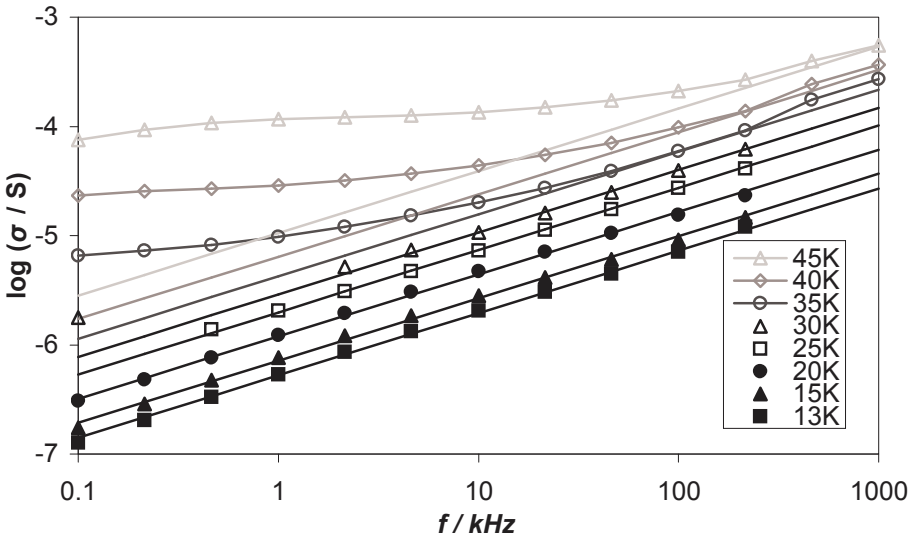

Figure 3.13: Frequency dependence of ac conductivity for various temperatures (13 K $\leq T \leq$ 45 K). Fits (straight lines) are calculated according to $\sigma \approx \omega^s$ model with a constant $s = 0.57$. Only the experimental data for $T < 35$ K are described accurately; for higher temperatures the experimental points deviate strongly from the model (curved lines in the upper part). Sample B1-1, $U_{ac} = 1$ V, $H_{dc} = 0$.

are plotted with respect to frequency of probing ac current. The straight lines correspond to the ω^s model and fit the experimental data accurately for low temperatures (in the lower part of the figure); the curved lines in the upper part of the figure join experimental points that deviate strongly from the fit (i.e. for $T = 35$, 40 and 45 K). It is also interesting to note, that the prefactors of the model - the $a(T)$ values of the Equation 3.1 very accurately follow an exponential law inbetween the Arrhenius' and the Mott's, specificaly $a(T) = a_0 \cdot \exp((E_a/k_B T)^{1/2})$. Even though the range of the $a(T)$ data is not particularly wide, it is evident from the data that neither Atthenius' (exponent 1) nor Mott's (exponent 1/4) mode describes the data precisely.

Based on the shape of the $\chi'(T)$ and $\varepsilon_r(T)$ dependencies one is tempted to compare the responsible processes. This is most easily done by comparing the

transition temperatures as functions of frequency for the magnetic glass-like transition ($T_g(f)$) and dielectric transition ($T_\varepsilon(f)$). These results are summarised in Figure 3.14. Again, the $T_\varepsilon(f)$ dependence can be described as Arrhenius' ther-

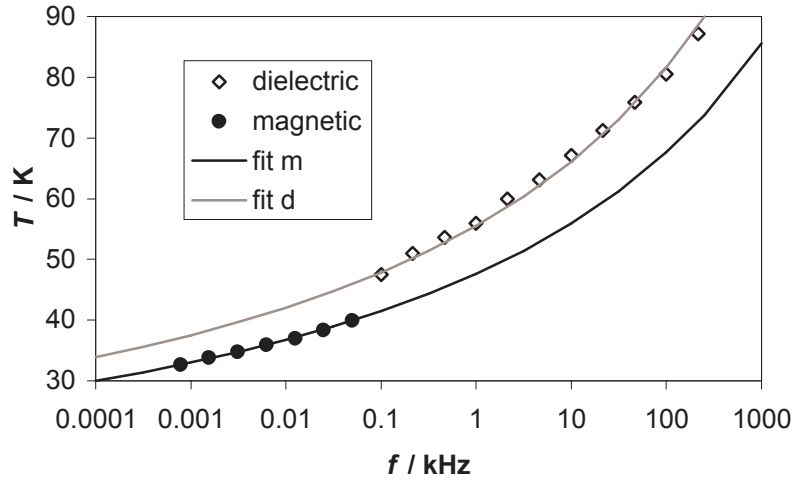

Figure 3.14: Comparison of the transition temperatures of the glass-like magnetic transition (the same data as in Figure 3.11) and dielectric permittivity transitions (extracted from the permittivity data in Figure 3.12) for accessible frequencies. The fitted activation energies E_a are 64 meV and 69 meV for the magnetic and dielectric transitions respectively. Sample B1-1, $U_{ac} = 1$ V, $H_{dc} = 0$, $\mu_0 H_{ac} = 5\ \mu$T.

mally activated process with the activation energy E_a slightly different from the energy associated with magnetic glass-like transition.

No significant frequency range overlap of magnetic and dielectric data could be achieved due to the limitations of the respective instruments, both the high-frequency magnetic susceptibility measurements and low-frequency dielectric measurements suffered from noise and large instrumental errors.

3.5 Low-temperature anomaly

From the Magnetic After-Effect (MAE) measurements of stoichiometric single crystal magnetite the existence of relaxation processed at low temperatures is well established. However, the striking discrepancy between the measured ac susceptibility in MAE experiments (see Figure 1.12) and that of conventional experiments (see e.g. Figure 3 in [64]) has not yet been addressed. This discrepancy is further illustrated in Figure 3.1, where at low temperatures (region denoted 'C') the susceptibility can achieve either 'low' value (as in a conventional measurement) or 'high' value (under certain conditions, e.g. periodical strong demagnetisation during the MAE experiment). The appearance and properties of this anomaly will be discussed below.

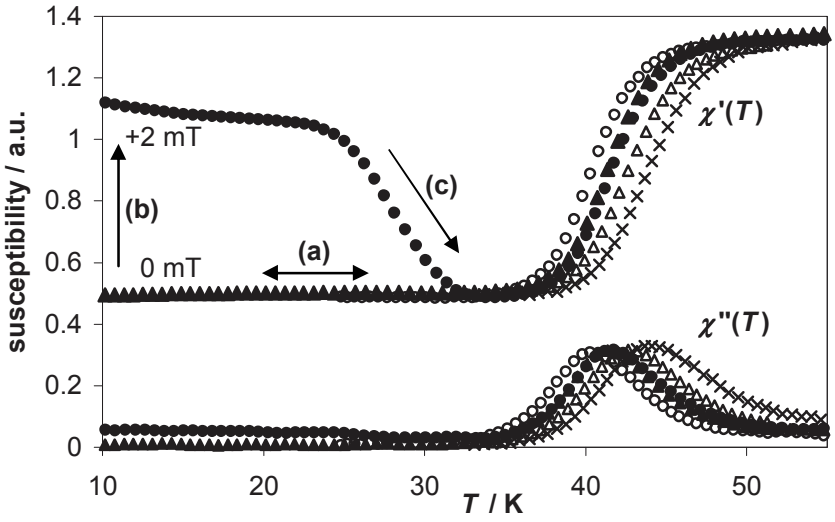

Figure 3.15: Real part (top symbols) and imaginary part (bottom symbols) of complex ac susceptibility as a function of temperature, ac field frequency 1.6 Hz (○), 3.1 Hz (●,▲), 6.3 Hz (△) and 12.5 Hz (×). The anomaly (●) was excited by increasing the dc field by 2 mT at 10 K. Sample H1, $\mu_0 H_{ac} = 5$ μT.

3.5.1 Novel relaxation phenomenon

Below about 30 K, when the magnetic moments responsible for glass-like transition are frozen-in for all practical frequencies, we measured and described a novel manifestation of relaxation processes in magnetite, the *low temperature anomaly* [23].

The low-temperature anomaly comes about in a manner described as follows: During cooling of a stoichiometric magnetite in a "normal" way (i.e. in relatively weak magnetic field without abrupt changes - ac field up to 100 μT and dc field up to several mT), χ' reaches its lowest value below the glass-like transition (further denoted as the "frozen" state) and retains this value down to the lowest temperatures (an arrow denoted (a) in Figure 3.15). Also, χ'' is nearly zero in this region. Upon subsequent warming at the same conditions, the same $\chi(T)$ is observed (symbols "▲" in Figure 3.15). However, when an abrupt disturbance is applied at low temperature (e.g. step change of dc field by several mT), χ' jumps to a new higher steady value, the anomaly is "excited" (an arrow denoted (b) in Figure 3.15). Upon subsequent warming of such excited sample, $\chi(T)$ relaxes back to the "frozen" state value before the glass-like transition takes place (an arrow denoted (c) in Figure 3.15). This universal behaviour of stoichiometric magnetite was found to be insensitive to the ac field frequency and amplitude (provided it is relatively weak, up to about 100 μT) and the absolute intensity of dc magnetic field (within our accessible range of +/- 20 mT). Only the magnitude and character of excitation event (even a short pulse of several mT amplitude may excite the anomaly) determines the extent to which the anomaly is excited.

To further explore this behaviour, we have performed an experiment in which the dc field was swept in a triangular fashion ($0 \rightarrow +1$mT $\rightarrow 0 \rightarrow$ -1mT $\rightarrow 0$ with a period of 120 s) with superimposed weak ac field (to facilitate ac susceptibility measurement) at several fixed temperatures (Figure 3.16). Apparently, at 35 K

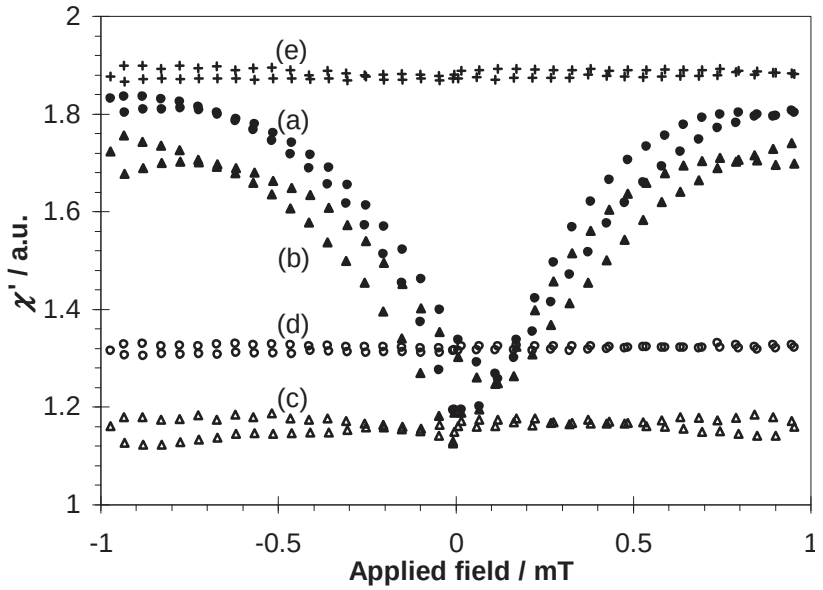

Figure 3.16: DC field dependence of ac susceptibility at various temperatures: (a) 10 K, (b) 28 K, (c) 35 K - the "frozen" state, (d) 43 K and (e) 50 K - above the glass-like transition. The field was swept continuously in the range of +/- 1 mT in a triangular fashion, the whole cycle taking 120 s. The susceptibility was measured simultaneously with an ac field of 20 μT at 6 Hz, H1 sample.

the sample maintained the "frozen" state regardless of the changing dc field (curve (c)). At lower temperatures the change of dc field causes χ' to increase, but in this case the process is largely reversible, and the sample returns close to the "frozen" state after removal of the dc field (curves (a), (b)). With other samples (H2, B1) or with bigger changes of the dc field the process is irreversible.

Changes of spontaneous magnetisation of magnetite sample during the transition are depicted in Figure 3.17. Although more dependent on the thermal and magnetic history of the sample, the magnetisation shows several general features: (i) no dramatic changes of magnetisation occur in the region of glass-like transition, neither on cooling nor on warming the sample, (ii) if the anomaly was excited at low temperature the sample fully accommodates to the new conditions by a change of spontaneous magnetisation that takes place at higher temperature than the relaxation of ac susceptibility (to the "frozen" state), and (iii) the magnitude of the change of spontaneous magnetisation is rather low, in this case only about 10% of the total response of the sample to the step change of the applied dc field.

The relaxation of the anomaly was also found to depend on the rate of sample warming: the lower the rate the lower the temperature at which the "frozen" state is reached. This feature is further explored in relaxation measurements where a step change of magnetic field is applied at a defined temperature in the range from 10 K to 35 K and the time dependence of the ac susceptibility is recorded (Figure 3.18).

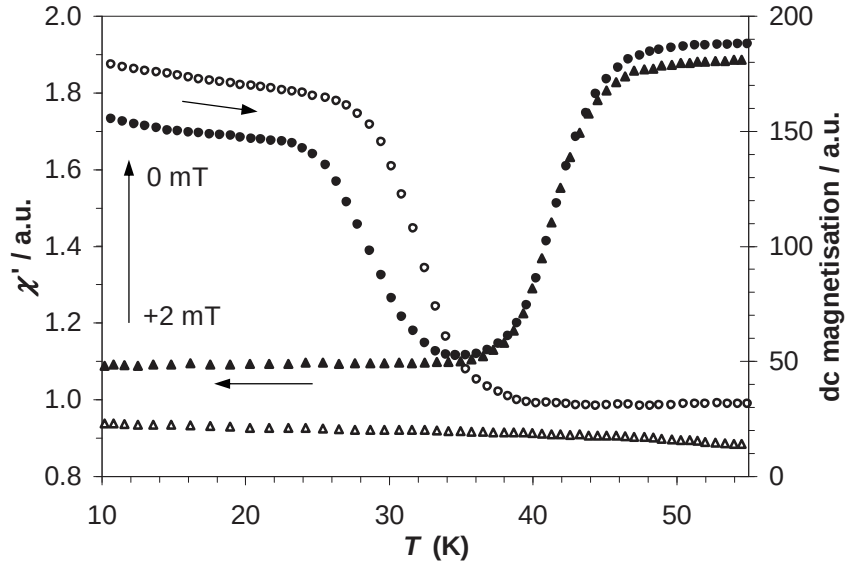

Figure 3.17: Real part of ac susceptibility (full symbols) and accompanying changes of spontaneous dc magnetisation (open symbols), H1 sample, as a function of temperature, ac field amplitude 5 μT at 6.3 Hz. The anomaly was excited by decreasing the dc field by 2 mT at 10 K. (The units of magnetisation are essentially A/m except for an additive constant - an offset - which is unknown due to working principle of a SQUID. This offset is also different for cooling ($\triangle$) and warming ($\circ$).)

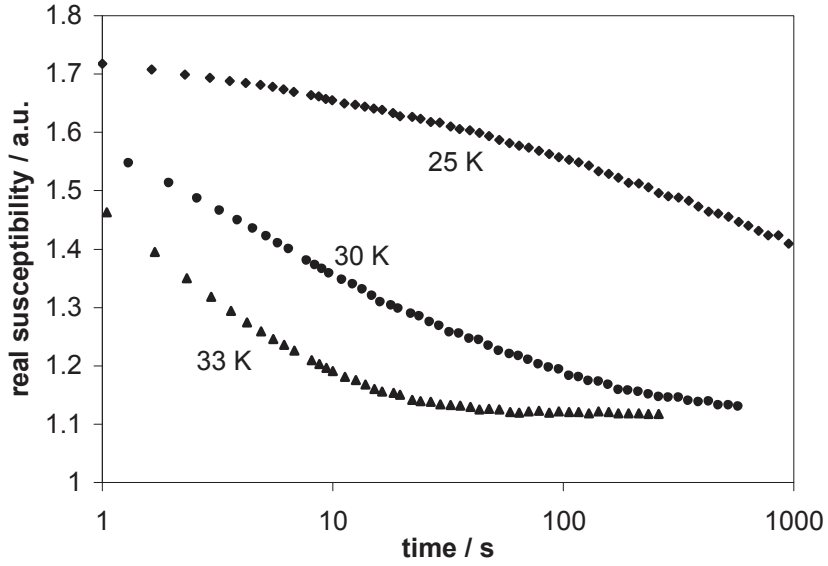

Figure 3.18: Relaxation of the real part of ac susceptibility after a 2 mT step of applied magnetic field at 25 K (top symbols), 30 K, and 33 K (bottom symbols). H1 sample, ac field amplitude 5 μT at 6.3 Hz.

The properties of several samples were measured and the results summarised in Table 3.2. Also in this case the differences in demagnetising factor among the samples may influence the exact position of the transition (see Section 1.1.5).

Table 3.2: A summary of the low-temperature anomaly transition temperatures T_a (warming rate 1 K/min) of measured samples. Ac amplitude was 10 μT, the anomaly was excited by a dc field step of 2 mT at 10 K. The transition temperatures are defined as inflection points of the $\chi'(T)$ curve. The differences in the magnitude of the anomaly (in percent of the magnitude of the glass-like transition) is mainly caused by different demagnetising factors of the samples.

sample	T_a / K	anomaly magnitude
H1	27.2	20 %
H2	23.0	80 %
B1	18.0	50 %

But due to the lack of any theoretical model this effect cannot be accurately evaluated.

3.5.2 Excitation of the anomaly

As already illustrated in Figure 3.16, symbols (a) and (b) (i.e. for temperatures below the low-temperature anomaly transition), the susceptibility increases quickly when the applied dc magnetic field is changed. In that particular case, however, after removing the field the susceptibility drops back to its 'frozen' state. This reversible behaviour is not an universal property of the anomaly, as can be seen from Figure 3.19, where the same experiment is performed in stronger field on two samples (B1 and H1) at low temperature. The susceptibility is expressed

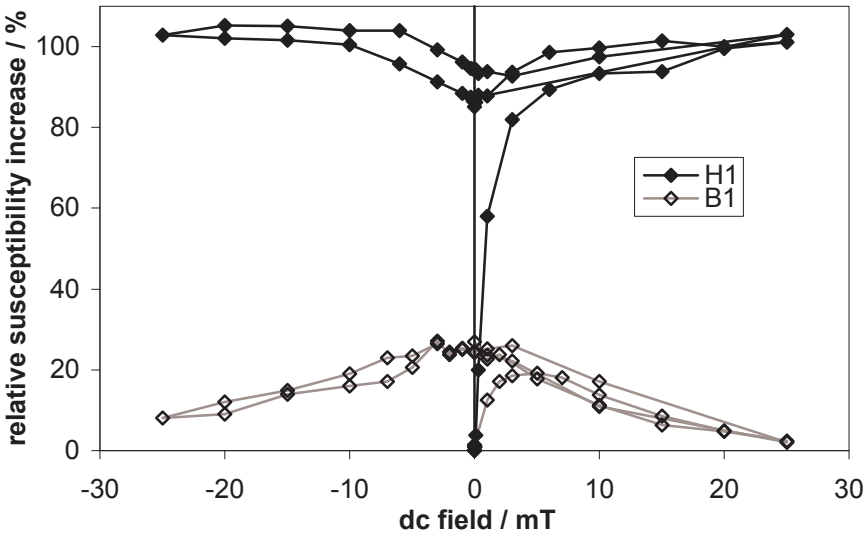

Figure 3.19: DC field dependence of ac susceptibility below the low-temperature anomaly transition, expressed as percentual fraction of the magnitude of respective glass-like transition. The field was changed step-wise in the range of ± 25 mT and allowed to relax until the susceptibility stabilised. Samples B1 and H1, $T = 10$ K, $\mu_0 H_{ac} = 20$ μT, $f = 6$ Hz.

as a difference (increase) from the 'frozen' state scaled as a percentage of the magnitude of the respective glass-like transition.

Due to the strong fields used in this measurement the applied dc magnetic field was adjusted step-wise and the $\chi'(t)$ was allowed to relax towards an equilibrium state (up to 100 seconds). Several findings are apparent from the plot:

1 - the $\chi'(H_a)$ is irreversible, it quickly attains higher value and never returns to the 'frozen' state (i.e. zero percent).

2 - the magnitude of the anomaly is 100 % in the case of H1 sample, whereas in the B1 sample the magnitude of the anomaly was roughly one fifth of the magnitude of the glass-like transition.

3 - in the case of B1 sample the susceptibility decreases in strong magnetic field.

Another feature, infrequently observed in stoichiometric magnetite samples, that pertains to the excitation of the low-temperature anomaly, is illustrated in Figure 3.20. Here the anomaly appeared during *cooling* in *constant dc field*. Both

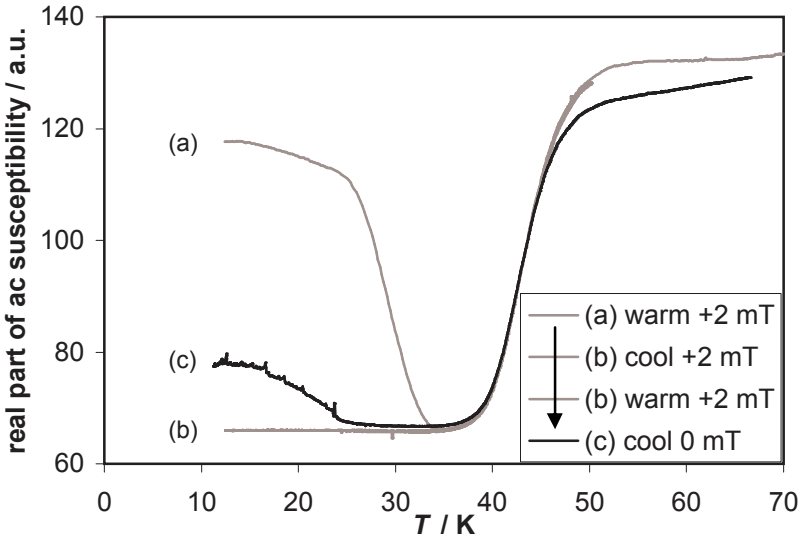

Figure 3.20: An example of anomaly excitation without altering the applied dc field. Curve (a) - warming in +2 mT field after cooling in zero field (i.e. normal procedure for anomaly excitation, as in Figure 3.15). Curves (b) - cooling and warming in +2 mT field, no anomaly excitation. Curve (c) - cooling in zero field, the anomaly appears during *cooling* and without changing the *dc field*; both these aspects do not fit into the description in Section 3.5.1. Sample H1, $\mu_0 H_{ac} = 10$ μT, $f = 6$ Hz.

these aspects contradict the description of the anomaly given above, as generally the anomaly can only be observed during *warming* after *changing the dc field*. This sort of memory-effect phenomenon was observed e.g. upon cooling in zero dc magnetic field after the sample was cycled through the anomaly transition temperature several times with applied field of 2 mT.

4. Results on doped magnetite

Due to the fact that preparation of non-stoichiometric high quality samples is even more challenging than the stoichiometric ones, especially in terms of homogeneity of distribution of lattice defects, some experimental features cannot be analysed in such depth and some features are missing at all. Thus this chapter is going to be significantly shorter than Chapter 3.

4.1 Samples overview

The samples used throughout this work are summarized in the Section 2.1. This chapter is devoted to non-stoichiometric single crystals of magnetite, again from two sources: samples denoted H from the laboratory of J. M. Honig and samples denoted B from V. A. M. Brabbers. The studied samples were annealed to non-stoichiometry $\delta = 0.002$, 0.0035 and 0.012 (defined as $Fe_{3(1-\delta)}O_4$). As explained in the Section 1.4.1, no natural magnetite samples were measured.

4.2 The Verwey transition

Figure 4.1 depicts the $\chi'(T)$ dependence for three non-stoichiometric magnetite single crystals in a temperature range around the Verwey transition. The width of the transition is apparently much larger and the Verwey transition temperature T_V is significantly lower than in the case of stoichiometric magnetite, however, an apparent hysteresis is still present. Moreover, the$\chi'(T)$ dependence for sample

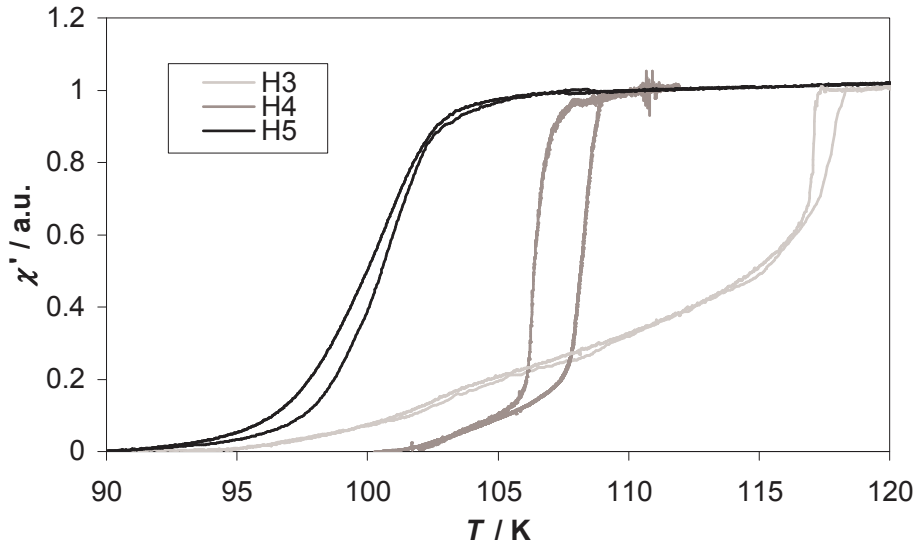

Figure 4.1: Temperature dependence of real part of complex ac susceptibility $\chi'(T)$ for three non-stoichiometric samples: H3 ($\delta = 0.002$, $T_V = 117.5$ K), H4 ($\delta = 0.0035$, $T_V = 107.2$ K) and H5 ($\delta = 0.012$, $T_V = 100$ K). $H_{dc} = 0$, $\mu_0 H_{ac} = 10$ μT.

H3 shows pronounced tail that spans 20 Kelvins, the other two samples posses a

tail that is shorter, about 5 K. This suggests non-homogeneous sample properties caused by a non-uniform vacancy distribution inside the samples. The transition was found to be insensitive to both the frequency and magnitude of probing ac magnetic field and the intensity of dc magnetic field, in the ranges accessible by our instrumentation.

The hysteresis, reviewed in detail in Figure 4.2 for sample H3, mainly occurs in the region in the upper part of the transition. The sample H4 displays similar behaviour, whereas sample H5, i.e. the one with highest departure from stoichiometry, does not show any appreciable hysteresis. It should be noted that the

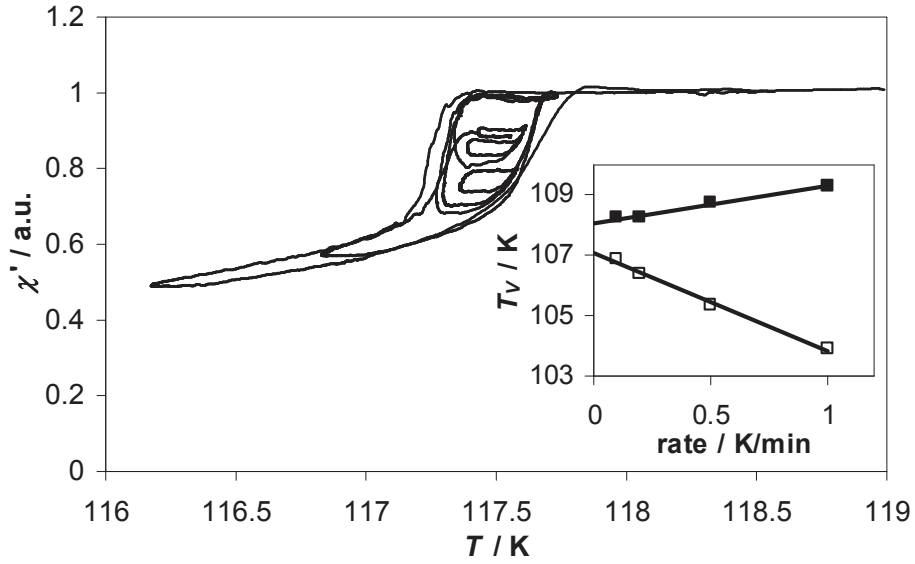

Figure 4.2: The detail of the temperature dependence of real part of complex ac susceptibility $\chi'(T)$ showing the hysteresis of the Verwey transition for sample H3. The scale of the susceptibility axis corresponds to that of Figure 4.1. The inset shows the dependence of the hysteresis of the transition on the rate of temperature change, sample H4. $H_{dc} = 0$, $\mu_0 H_{ac} = 10\ \mu$T.

extrapolated limiting hysteresis of the Verwey transition (the inset of Figure 4.2) is about 0.8 K in sample H4, which is larger than hysteresis in stoichiometric samples (see inset of Figure 3.4).

4.3 Glass-like transition

Similarly to stoichiometric samples, the non-stoichiometric ones also display a glass-like transition, see Figure 4.3. It is a frequency dependent transition, that

is not sensitiove to the magnitudes of ac and dc magntic fields (in the ranges accessible by our instrumentation).

Unlike for the stoichiometric samples, however, in this case the Debye's model (see Section 1.1.5) does not fit to the experimental data. Nevertheless, the transition temperatures T_g can be estimated from the points of inflexion of the $\chi'(T)$ curves or from the peaks of the $\chi''(T)$ curves and plotted versus frequency of ac field. This is illustrated in Figure 4.4, together with attempts to fit the

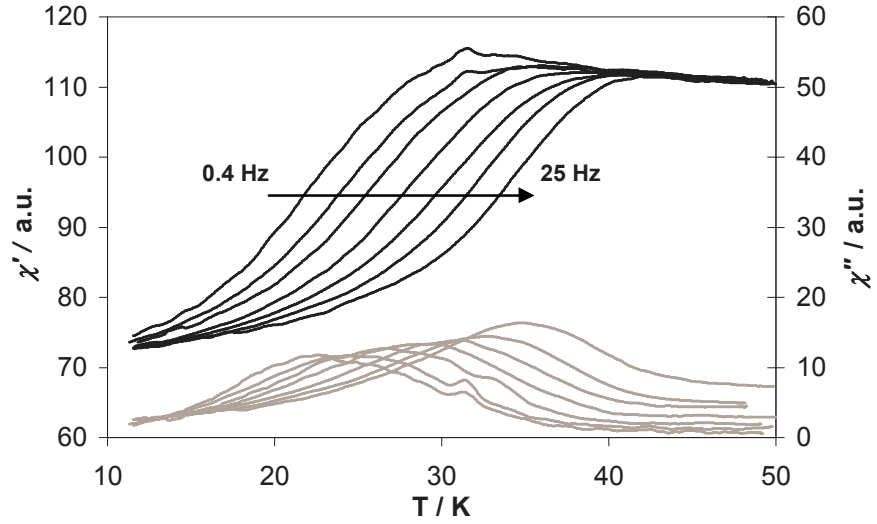

Figure 4.3: Temperature dependence of real part (black lines, left axis) and imaginary part (gray lines, right axis) of ac magnetic susceptibility for frequencies $f = 0.4, 0.8, 1.5, 3.1, 6.3, 12.5, 25$ Hz. Sample H3, $\mu_0 H_{ac} = 5\ \mu$T, $H_{dc} = 0$.

experimental $T_g(f)$ data with an exponential Arrhenius' fit. The parameters of

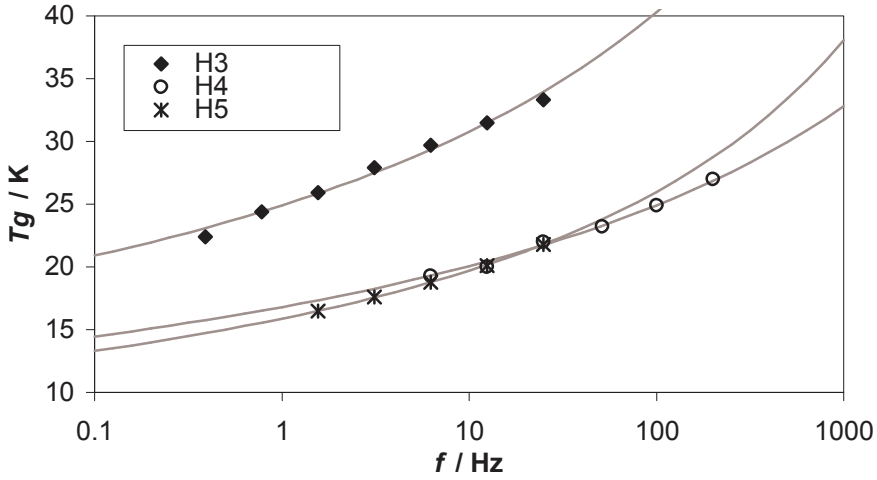

Figure 4.4: A compilation of the transition temperatures of the glass-like transitions T_g versus frequency for non-stoichiometric magnetite samples. The points are experimental data (points of inflexion on the $\chi'(T)$ curves), the lines are exponential Arrhenius fits in reasonable agreement with the datapoints. $\mu_0 H_{ac} = 5\ \mu$T, $H_{dc} = 0$.

the exponential models are summarised in Table 4.1. Compared with a similar table for stoichiometric samples (Table 3.1), one notes that the time constants are several orders of magnitude larger.

Table 4.1: A summary of activation parameters associated with the glass-like transition in non-stoichiometric magnetite samples. The parameter τ of the measured Debye-like relaxation of complex ac susceptibility is approximated by an exponential Arrhenius temperature-activated process, i.e. $\tau(T) = \tau_0 \exp(E_a/k_B T)$, here E_a is and activation energy and τ_0 is a time constant (attempt period).

sample	E_a / meV	τ_0 / ns
H3 ($\delta = 0.002$)	26	5800
H4 ($\delta = 0.0035$)	21	710
H5 ($\delta = 0.012$)	16	7100

4.4 Low-temperature anomaly

As we have observed in the case of stoichiometric high quality single crystals of magnetite, the characteristic temperatures of both the glass-like transition and the onset of the low-temperature anomaly are extremely sensitive to the sample quality. Even in the case of 'stoichiometric' samples the temperatures may differ by more than 10 K (See Table 5.1). Even the least doped or least non-stoichiometric samples available to us were too far from stoichiometry that the anomaly could not be observed even at the lowest attainable temperature (about 5 K, see Figures ref-glass-like-transitions-doped), and very likely these effects would not appear down to 0 K. This is also apparent from Figure 4.3, where the glass transition spans well below 15 K.

5. Discussion

We have performed a detailed experimental study of the behaviour of various magnetite samples in weak magnetic and electric fields in the temperature range from 6 to 130 K. The experimental results obtained on stoichiometric (see Chapter 3) and doped (see Chapter 4) single crystals of magnetite form the main body of this thesis. As the experimental data are dealing with distinct features of magnetite (magnetic measurements of the Verwey transition, low-temperature behaviour, dielectric measurements in wide temperature range below T_V), the discussion will be divided accordingly. The main focus of the discussion will be the newly observed anomalous magnetic low-temperature behaviour of magnetite and its correlation with dielectric measurements.

5.1 The Verwey transition

The Verwey transition is a structural phase transition accompanied by a sharp change of magletocrystalline anisotropy and electrical conductivity. In the case of stoichiometric sample we have shown the first-order character of the transition by a simple measurement of partially thermally insulated sample and subsequent comparison of the measured $T(t)$ dependence to a simple numerical model (see Figure 3.3). The model has only two free parameters: the thermal conductivity between the sample and the sample holder and the latent heat of the transition, thus the perfect fit suggest that the assumption of first-order transition is appropriate.

The calculated value of the latent heat of H2 sample $L = 0.63 \pm 0.1$ kJ mol^{-1} (the uncertainty coming mainly from the variation of the value of the specific heat of magnetite near T_V as found in the literature) fits perfectly into the range of values measured by more elaborate methods [34].

From the magnetic point of view it is worth noting that we have observed random fluctuations of spontaneous magnetisation in stoichiometric magnetite samples during the Verwey transition, i.e. during the period when the sample temperature is kept constant by the absorption or evolution of latent heat (see Figure 3.2). These fluctuations probably arise from the interaction between structural and magnetic domains. More specifically, on cooling through T_V the monocrystalline sample splits into structural domains, each having its c axis aligned along one of the cubic axes of the high-temperature structure. As the new low-temperature structure has a preferred orientation of magnetisation, the progressing structural transformation will be accompanied by changes of total spontaneous magnetisation. On the other hand, during the transformation also the effects of magnetostatic interactions must be considered when minimising the potential energy of the system, thus one can for example force the sample into preferred crystal orientation by cooling through T_V in strong magnetic field.

The magnetic susceptibility measurements of the Verwey transition (see e.g. region A in Figure 3.1) reveal a number of properties: 1) The transition is very sharp and it is possible to precisely determine the critical temperature of the transition T_V. This temperature is an important measure of sample quality (see

Figure 1.9 and Table 5.1, where the main measured properties of the studied samples are summarised). 2) The susceptibility below T_V is low ($\chi = 1$ to 2), whereas it is high above T_V (χ is as high as 10^3), this is caused by strong magnetocrystalline anisotropy that results from the lowering of symmetry below the transition. Another important point here is that the measured susceptibility is close to the intrinsic one below T_V, but above T_V the measured value is limited to $1/D$, where D is the demagnetising factor (see Section 1.1.4). Thus the ac magnetic susceptibility cannot be measured reliably above T_V, unless special methods to minimise demagnetisation are used (see e.g. Figure 1.11). 3) The Verwey transition is independent of the magnitude of the applied ac and dc magnetic fields and the ac field frequency in the range accessible by our instruments (magnetic field up to 20 mT and frequency up to 200 Hz). 4) Even slightly non-stoichiometric samples displayed widening of the transition and signs of multiple transitions, a clear indication of inhomogeneous distribution of dopants. These non-stoichiometric samples are not suitable for detailed analysis.

Table 5.1: A summary of magnetite samples used through this experimental work together with their basic properties. The non-stoichiometry is expressed as $Fe_{3(1-\delta)}O_4$. The T_V is defined as the midpoint of the $\chi'(T)$ dependence, the glass-like transition T_g is defined as the inflexion point of the $\chi'(T)$ dependence at a measuring frequency of 6.25 Hz and the temperature of the relaxation of the low-temperature anomaly T_a is defined as the peak of the $\mathrm{d}/\mathrm{d}T\ \chi'(T)$ dependence while warming at 1 K/min.

sample	δ 10^{-3}	T_V (K)	T_g @ 6.25 Hz (K)	T_a @ 1 K min^{-1} (K)	anomaly magnitude
H1	0	122.2 ± 0.3	42.7 ± 0.4	28 ± 2	100 %
H2	0	122.0 ± 0.3	40.1 ± 0.5	23 ± 2	20 %
B1	0	121.5 ± 0.3	35.9 ± 0.6	18 ± 2	50 %
B1-1	0	121.5 ± 0.3	34.8 ± 0.7	17 ± 2	20 %
H3	2	117.5 ± 0.5	29.4 ± 0.9	–	–
H4	3.5	107.2 ± 0.5	19 ± 1	–	–
H5	12	100 ± 1	19 ± 1	–	–

We also attempted to measure the dielectric properties of magnetite. We observed the nearly two orders of magnitude change of electrical conductivity on passing the transition (see Figure 3.9), but due to the high conductivity both above and below the transition the displacement current could not be measured, so the dielectric permittivity cannot be calculated. The real part of the conductivity was found to be independent of measuring frequency above 110 K (in the range from 20 Hz to 1 MHz). Due to low quality of the non-stoichiometric samples they were not subject to the dielectric measurements.

5.2 Low-temperature magnetic behaviour of magnetite

As was explained in the above paragraphs the magnetic and dielectric measurements of the Verwey transition can reveal only limited amount of information. On the other hand, similar measurements at lower temperatures reveal a number of interesting phenomena. From the point of view of magnetic measurements this is mainly due to frequency and time dependence of relaxation processes that are observable by our instruments, and due to the fact, that the magnetic susceptibility is low and demagnetising effects do not distort the measured values significantly.

There is strong evidence that the magnetic susceptibility of magnetite at low temperatures originates mainly from the domain walls. The supporting arguments are following:

(i) Both the saturation magnetisation ($4\mu_B$ per Fe_3O_4 formula agrees well with the experimental value of 0.5 MA/m [53] (see Figure 1.7) and the magnetocrystalline anisotropy (the largest component [13] is about 0.25 MJ/m^3, see Figure 1.4) are fairly constant below T_V. Thus the susceptibility arising from the rotation of domain magnetisation should not depend on temperature.

(ii) The susceptibility arising from domain wall rotation is about an order of magnitude lower [39] than the measured susceptibility.

(iii) Susceptibility measurements in high dc magnetic field [5] show rapid decrease of ac susceptibility with increasing dc field applied during cooling through T_V, caused by the reduction of the number of magnetic domains.

In accordance with MAE measurements performed on high-quality stoichiometric magnetite single crystals [74] (see Figure 1.12), we identified two temperature regions where relaxation processes appear. These are the glass-like transition and the low-temperature anomaly.

5.2.1 Glass-like transition

Glass like transition is a Debye-like transition of ac magnetic susceptibility (see Figure 3.10). Both the real and imaginary part of the transition agrees well with the general shape of the Debye transition (see Section 1.1.5 for reference of the Debye model). The transition is strongly frequency-dependent, the temperature dependence of the transition frequency f_t being exponential (see Figure 5.1). Due to rather small range of frequencies that can be measured with our magnetometer the exact exponent parameter n of the dependence $f_t = f_0 \exp(T/T_0)^n$ cannot be extracted reliably, though the Arrhenius model ($n = 1$) gives good fit for both stoichiometric and doped samples. The Arrhenius parameters that describe the temperature activation of the glass-like transition in the measured samples are summarised in Table 5.2. An apparent conclusion from the analysis of the thermal activation associated with the glass-like transition is that the activation energy

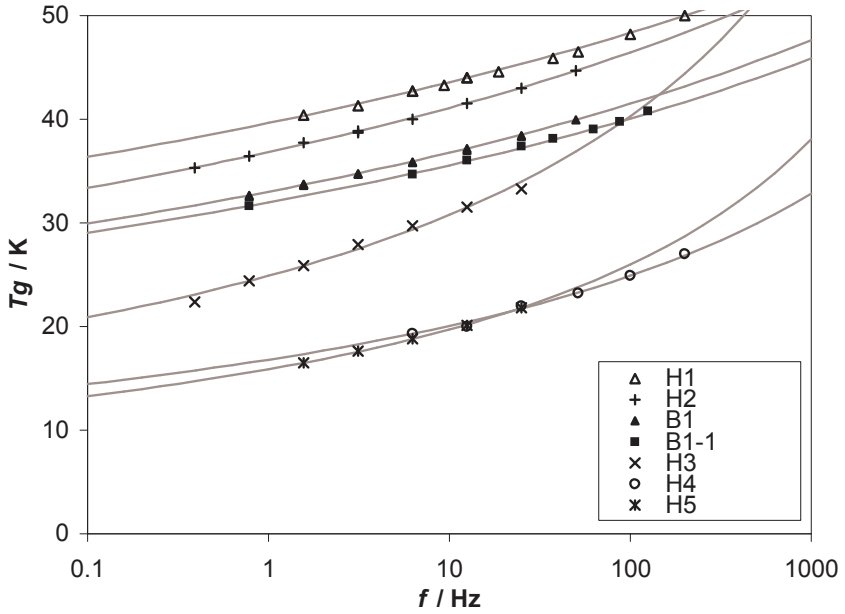

Figure 5.1: A compilation of the transition temperatures of the glass-like transitions T_g versus frequency for various stoichiometric and non-stoichiometric magnetite samples. The points are experimental data (points of inflexion on the $\chi'(T)$ curves), the lines are exponential Arrhenius fits, apparently describing the data quite well. $\mu_0 H_{ac} = 5\mu\mathrm{T}$, $H_{dc} = 0$.

Table 5.2: A summary of activation parameters associated with the glass-like transition in stoichiometric and non-stoichiometric magnetite samples. The parameter τ of the measured Debye-like relaxation of complex ac susceptibility is approximated by an exponential Arrhenius temperature-activated process, i.e. $\tau(T) = \tau_0 \exp(E_a/k_B T)$, here E_a is and activation energy and τ_0 is a time constant.

sample	E_a / meV	τ_0 / ns
H1	87	0.0079
H2	71	0.22
B1	64	0.17
B1-1	63	0.13
H3 ($\delta = 0.002$)	26	5800
H4 ($\delta = 0.0035$)	21	710
H5 ($\delta = 0.012$)	16	7100

E_a is significantly lower for doped samples and the numerical prefactor τ_0 is larger (by more than four orders of magnitude) for doped samples. The H1 sample can be regarded as of the highest quality among the studied samples.

As the magnetic manifestation of the transition is expected to come from the domain walls, the glass-like transition can be described as a freezing of domain walls: during cooling through the transition the mobility of the domain walls decreases and their ability to track the changing ac magnetic field (at given frequency) gradually vanishes. This gives rise to the typical sigmoid shape of the $\chi'(T)$ dependence accompanied by an absorption peak.

The magnitude of the change of susceptibility $\Delta\chi'$ during the transition was found to be independent on the applied dc magnetic field in the range of ± 20 mT, but in stronger magnetic fields it is known to vanish [5], consistently with the reduction of the number of magnetic domain walls by the DC field. The glass-like transition is also extremely sensitive to the quality of samples, as can be clearly seen from Table 5.1. It is also worth noting here that the ever-present demagnetising effects not only decrease the apparent susceptibility but also shifts the transition temperature of the Debye transition towards higher temperatures (for the detailed calculations see Section 1.1.5). Taking into account the actual values of magnetic susceptibility below T_V, this effect is less than 0.5 K for demagnetising factor $D = 1/2$.

5.2.2 Low-temperature anomaly

We have noticed a striking difference between the ac susceptibilities accompanying magnetic after-effect studies (MAE, disaccommodation effect) of stoichiometric magnetite [74] and the susceptibilities measured by other techniques (e.g. an inductive bridge method [64]) below 35 K. This ambiguity is shown schematically in the region C of Figure 3.1 as a bifurcation of the $\chi'(T)$ dependence. More specifically, MAE measurements produce the upper curve (i.e. upon cooling the susceptibility starts to rise again); conventional measurements produce the lower curve (i.e. the susceptibility is constant below the glass-like transition). Detailed susceptibility measurements of this temperature region revealed an unexpected behaviour which we term *the low-temperature anomaly*.

The results of magnetic susceptibility measurements of high-quality single crystals of magnetite presented in Section 3.5 show that magnetite can be excited to the high-susceptibility state by application of step change of dc magnetic field (several mT in magnitude) at low temperature (see Figure 3.15). During MAE experiments the sample is periodically excited by strong magnetic pulses, thus the anomaly is inevitably found in its excited state.

Here we present a simple microscopic model of the anomaly, taking into account the arguments summarised above and assuming these effects originate from domain walls: to explain the low-temperature phenomena we hypothesise the existence of pinning centres that create a net of potential minima for the domain walls. Starting from the "frozen" state at 35 K (see Figure 3.15) all domain walls lie in these minima, and a weak applied ac field induces only a small response of the sample magnetisation, χ' is small. According to the assumptions [66] about domain wall parameters we may assume that an ac field with amplitude $\mu_0 H_{ac} \leq 100$ μT is weak enough to cause domain wall displacement that is much less than the wall thickness. This process is reversible and, if the pinning centres are stationary, no energy is dissipated (χ'' is also small). But as the temperature is elevated the pinning centres are no longer fixed, thermal activation allows them to follow the displacing walls, and energy is dissipated. This process gives rise to the frequency-dependent Debye-like relaxation at 40 - 50 K as described in previous sections. Above 60 K the pinning centres move freely with the domain walls, the potential minima are not effective, and χ' is large.

To complete the explanation of the anomaly let us again start from the "frozen" state at 35 K, where the domain walls reside in their potential min-

ima. This state is preserved when the sample is further cooled to the lowest temperature (6 K in our experiments). Now the anomaly can be "excited", e.g., by changing the dc component of the applied magnetic field by a sizable amount (several mT). The domain walls are pulled from their potential minima and χ' rises (see curve (a) in Figure 3.16). The frozen pinning centres cannot rearrange according to the new magnetic domain pattern, so the sample remains in the excited state indefinitely (here we note that under some conditions, like weak dc field step, the excitation may be reversible, i.e. the susceptibility returns to its lower value after returning the dc field to its previous level, as in Figure 3.16). When this "excited" sample is warmed gradually, the hypothetical pinning centres start to move to their new equilibrium positions, i.e. into the domain walls, new potential minima appear and the susceptibility approaches the "frozen" state. This gives rise to strongly temperature-dependent relaxation of the ac susceptibility (see Figure 3.18), and the very same relaxation is responsible for the large peak in MAE spectra at about 30 K [74].

The microscopic nature of the hypothesised pinning centres remains unclear. However, some arguments can be summarised to elucidate the underlying mechanism: (i) a similar effect in iron [67] is ascribed to the diffusion of impurities (at concentration of 0.01%). This most definitely will *not* be the case of magnetite, as even minute concentration of impurities or structural defects shifts the glass-like transition to lower temperatures (in accordance with MAE results [73]) and destroys the low-temperature anomaly (see Table 5.1 for the exceptional sensitivity to sample quality). Also, relaxation effects of vacancies and impurities in magnetite are expected well above T_V. (ii) The crystallographic domains that appear when cooling magnetite single crystal through T_V have a substantial impact on the magnetic susceptibility [5], but their structure is fixed at low temperature (easy axis switching can be induced by much larger fields close below T_V [36]) and the structural domains themselves cannot account for the observed phenomena.

One plausible explanation is the interplay between the structural, magnetic and ferroelectric domain structure, as spontaneous polarisation was identified in magnetite thin films below 40 K [1] and the coupling between magnetic and dielectric properties of magnetite was identified long ago [58]. Other possible process responsible for this effect is the rearrangement of electrons along the B-sublattice (refer to Section 1.3) inside the domain wall (i.e. in the region where the saturated magnetic field is rotated out of the easy direction). As the relaxation time of this process should be of the order of the time / frequency scale of the anomaly and glass-like transition measurements (nearly zero to 100 Hz in the temperature range of our magnetic measurements), the relaxations can possibly be detected by dielectric measurements (discussed in one of the following chapters). Additionally, one may get more detailed information about these low-temperature magnetic processes through studying the nonlinear nature of the $\chi(T)$ in this region, which can be conveniently performed by measurements of higher harmonics of ac magnetic susceptibility (see Section 1.1.3).

5.3 Transport properties of magnetite below the Verwey transition

We performed both dc and ac electrical conductivity measurements on several stoichiometric magnetite samples in wide temperature range to decide among various models of dc conductivity and to probe for electronic relaxation phenomena linked to the magnetic glass-like and anomalous transitions.

5.3.1 DC electric conductivity of magnetite

In the measured range from 30 to 120 K the dc conductivity of magnetite changes by 10 orders of magnitude. In the low conductivity range we used a constant voltage method, where a voltage of 2 V was applied and the current measured by an electrometer. At higher temperatures standard laboratory multimeter was used to measure the conductivity using constant current method (0.5 μA to 1 mA), the current had to be changed several times to operate the instrument in favourable condition, i.e. the voltage drop developped across the sample was kept to 0.1 to 5 V. These results are summarised in Figure 3.7. The discontinuities associated with the changes of electric current suggest a nonlinear $V(I)$ characteristic of the sample, which was confirmed by sweep measurements (see Figure 3.8), indicating non-linear behaviour in the range from 60 to 250 K (in the range from 90 to 140 K the small-signal (100 mV) conductivity was at least ten times lower than the differential conductivity at 5 V).

The wide temperature range of the measurement allows us to reliably determine the exponent of the temperature dependence of electrical resistivity according to the exponential model

$$\rho = \rho_0 \mathrm{e}^{-(T_0/T)^n} \ , \tag{5.1}$$

where $n = 1$ corresponds to Arrhenius temperature activation, $n = 1/4$ is the Mott's variable range hopping model of dc conductivity (see Section 1.2.2), $n = -1$ is simple exponential dependence. Whereas some authors found a piecewise Mott's [74] or Arrhenius' dependence, or found the Mott's dependence applies only in a certain temperature range [61], our data suggest the validity of a single Mott's model over the whole measured temperature range. The activation constant $T_0 = 10^8$ K falls within the range of values typical for amorphous tetragonal semiconductors (as noted in [42]).

We also confirmed the change of dc conductivity at the Verwey transition of about two orders of magnitude (refer to Figure 3.9). The conductivity at and above T_V was too high and didn't allow for more detailed analysis.

5.3.2 AC dielectric properties of magnetite

In order to shed more light on the nature of the low-temperature relaxation processes in magnetite we also performed ac dielectric measurements on stoichiometric samples in the range from 100 Hz to 1 MHz. Due to the limitations of the instrumentation and the broad range of conductivities that had to be measured neither constant-current nor constant voltage scheme could be used, but a combination of both. The complex ac conductivity was expressed in terms of resistive

and capacitive component (parallel RC model) and due to the favourable sample geometry (a disc with opposing planar electrodes) these components were scaled to represent the intrinsic conductivity and permittivity of the material.

Immediately apparent from Figure 3.12 is the high value of relative permittivity (as high as $2 \cdot 10^4$) that suggest an inhomogeneous charge distribution [41]. As the effect of the space charge associated with electrodes is expected at lower temperatures (around 10 K [32]), the high permittivity could result from intrinsic inhomogeneities, such as the structural or magnetic domain walls.

The real part of ac electric conductivity is higher than the dc limiting value and obeys an empirical ω^s model at temperatures below 35 K ($s = 0.57$), see Figure 3.13. This frequency dependence of conductivity is often observed in disordered semiconductors [42], i.e. in materials with broad distributions of relaxation times.

The main motivation for performing the dielectric measurements was the possibility to explain the microscopic nature of the glass-like transition and the low-temperature anomaly. As discussed above these magnetic effects can be caused by slow electronic relaxations and these may be also observable in dielectric spectroscopy measurements. Indeed, the $\varepsilon_r(T)$ dependences at various frequencies (Figure 3.12) is remarkably similar to the $\chi'(T)$ curves of the glass-like transition (Figure 3.10). A more quantitative comparison is given in Figure 3.14 where the frequency dependence of the transition temperatures of the dielectric and glass-like transitions are summarised. While both these datasets follow Arrhenius' dependence with nearly equal activation energies ($E_a = 66 \pm 3$ meV), the prefactors differ by a factor of four (at given temperature the transition frequency of the glass-like transition is four times higher than the transition frequency of the dielectric permittivity).

Here we note that we didn't try to extract the exponential factor from the experimental $T(f)$ data; we assumed the Arrhenis' dependence as the simplest case. Wider frequency range would be necessary to fit the exponential factor with any certainty.

Conclusion

We present detailed magnetic and transport measurements of numerous high-quality magnetite samples in weak magnetic and electric fields, together with basic theoretical and experimental overview necessary for their discussion, supplemented by in-depth overview of the involved experimental methods.

In the part dedicated to the magnetic measurements we focused on ac susceptibility measurements in three temperature regions according to the most prominent phenomena that take place in distinct temperature ranges: the region of the Verwey transition around 120 K, the region of the glass-like transition at about 30 K to 60 K and the region of the low-temperature anomaly below 30 K.

In the Verwey region we present detailed measurements of the transition together with a discussion of the limitations of such measurements by demagnetising effects, we support the first-order nature of the transition by measuring the latent heat and showing coexistence of phases and thermal hysteresis, spontaneous magnetic fluctuations during the transition, and finally we emphasize the influence of sample stoichiometry and quality on the general properties of the Verwey transition.

At lower temperatures a strongly frequency-dependent glass-like transition is studied experimentally and an empirical model of Debye transition with Arrhenius' temperature activation is successfully applied to the data obtained on stoichiometric samples. Notable is the high sensitivity of this transition on sample quality, in the studied samples the temperature shift was about five times larger than the shift of T_V, thus even nominally stoichiometric samples can be reliably distinguished based on their quality.

We have noted a striking discrepancy between the results of ac susceptibility measurements using different methods, which brought us to the observation of a novel relaxation phenomenon, a low-temperature anomaly, where the susceptibility depends strongly on the thermal and magnetic treatment and shows thermally dependent relaxation. We consistently explained this behaviour (and the glass-like transition as well) as a temperature-dependent diffusion of hypothetical pinning centres towards the magnetic domain walls. The nature of this pinning sites is unknown but several mechanisms are excluded, such as impurities or vacancies, based on their relaxation rates and the exceptional sensitivity of the anomaly to sample quality (generally it can be observed only in stoichiometric samples). Some sort of domain pattern may be the cause of the pinning (excluding structural domains which are fixed at these temperatures), alternatively, an electronic process may be responsible.

In the part dedicated to electrical measurements we present dc conductivity measurements and ac dielectric spectroscopy in rather wide temperature and frequency range. Apart from the two orders of magnitude jump of dc electric conductivity encountered upon traversing the Verwey transition we also observed ten orders of magnitude range of conductivity from T_V down to 13 K. We successfully applied Mott's variable-range hopping model to the $\sigma_{dc}(T)$ data in the whole temperature range and determined the Mott's exponent (1/4) with high confidence (0.26 ± 0.03). We also recorded nonlinear voltage-current character-

istics, an indication of heterogeneous semiconductor nature of magnetite, both below and above T_V.

The dielectric measurements were motivated by the observed anomalous magnetic behaviour, which could be explained on the basis of electronic relaxations. We present the results as a parallel RC model in terms of the intrinsic conductivity and permittivity. The ac conductivity is higher than its dc limit and approaches an ω^s model below 35 K, reminiscent of the behaviour of disordered semiconductors.

The most notable feature of the dielectric permittivity is its extremely high value at certain temperatures and frequencies, most likely caused by space charge accumulation on internal heterogeneities. The transition of the permittivity is also strongly frequency dependent, similarly to the magnetic glass-like transition, obeys the Arrhenius' relation with nearly identical activation energy but differs in the frequency prefactor. Based on the presented experimental findings we cannot conclusively decide whether the magnetic domain wall pinning mechanism and the dielectric response originate from the same microscopic process.

Finally, we once again emphasize the importance of high quality stoichiometric single-crystalline samples, as these can provide much more information than doped or non-stoichiometric samples, where the inevitable inhomogeneous distribution of impurities smears out important features. As an example, the low-temperature magnetic anomaly can only be observed in the best available stoichiometric samples.

Bibliography

[1] Marin Alexe, Michael Ziese, Dietrich Hesse, Pablo Esquinazi, Kunihiko Yamauchi, Tetsuya Fukushima, Silvia Picozzi, and Ulrich Gosele. Ferroelectric switching in multiferroic magnetite (Fe_3O_4) thin films. *Advanced Materials*, 21(44):4452–4455, 2009. ISSN 1521-4095.

[2] P. W. Anderson. Ordering and antiferromagnetism in ferrites. *Phys. Rev.*, 102:1008–1013, May 1956.

[3] P. W. Anderson. Absence of diffusion in certain random lattices. *Phys. Rev.*, 109:1492–1505, Mar 1958.

[4] I.G. Austin and N.F. Mott. Polarons in crystalline and non-crystalline materials. *Advances in Physics*, 18(71):41–102, 1969.

[5] M. Balanda, A. Wiecheć, D. Kim, Z. Kąkol, A. Kozłowski, P. Niedziela, J. Sabol, Z. Tarnawski, and J. M. Honig. Magnetic ac susceptibility of stoichiometric and low zinc doped magnetite single crystals. *Eur. Phys. J. B*, 43(2):201–212, 2005.

[6] L. R. Bickford. Ferromagnetic resonance absorption in magnetite single crystals. *Phys. Rev.*, 78:449–457, May 1950.

[7] L. R. Bickford, J. M. Brownlow, and R. F. Penoyer. Magnetocrystalline anisotropy in cobalt-substituted magnetite single crystals. *Proceedings of the IEEE. Institute of Electrical and Electronics Engineers*, B104:238–244, 1957.

[8] M. Blackman, G. Haigh, and N. D. Lisgarten. On the magnetic transformation and the domain structure of magnetite. *Proceedings of the Physics Society*, 81:244, 1963.

[9] F. Bloch. Zur Theorie des Austauschproblems und der Remanenzerscheinung der Ferromagnetika. *Zeitschrift fur Physik*, 74:295–335, May 1932. doi: 10.1007/BF01337791.

[10] V. A. M. Brabers. The preparation of tetragonal single crystals in the $Mn_xFe_{3-x}O_4$ system. *Journal of Crystal Growth*, 8(1):26 – 28, 1971. ISSN 0022-0248.

[11] James J. Brophy. Magnetic fluctuations in molybdenum permalloy. *Journal of Applied Physics*, 29(3):483–484, 1958. doi: 10.1063/1.1723189.

[12] P. N. Butcher, K. J. Haydek, and J. A. McInnes. Analytical formulae for d.c. hopping conductivity. *Phil. Mag.*, 36:19–32, 1977.

[13] K. Chiba and S. Chikazumi. Magnetocrystalline anisotropy of magnetite. *Journal of Magnetism and Magnetic Materials*, 31-34, Part 2(0):813 – 814, 1983. ISSN 0304-8853.

[14] D. J. Craik. Domain theory and observation. *Journal of Applied Physics*, 38 (3):931–938, 1967.

[15] C. de Francisco, J. Iniguez, J. Munoz, and J. Ayala. Automatic disaccommodation measuring system. *IEEE Transactions on Magnetics*, 23:1866–1868, 1987.

[16] F. Edgar, Jr Westrum, and F. Gronvold. Magnetite (Fe_3O_4) heat capacity and thermodynamic properties from 5 to 350 K, low-temperature transition. *The Journal of Chemical Thermodynamics*, 1(6):543 – 557, 1969. ISSN 0021-9614.

[17] S. R. Elliott. A.c. conduction in amorphous chalcogenide and pnictide semiconductors. *Advances in Physics*, 36(2):135–217, 1987.

[18] T. Fujii, M. Takano, R. Katano, Y. Bando, and Y. Isozumi. CEMS study of the growth and properties of Fe_3O_4 films. *Journal of Crystal Growth*, 99(1-4, Part 1):606–610, Jan 1990. ISSN 0022-0248. doi: 10.1016/0022-0248(90)90592-9.

[19] Joaquin García and Gloria Subías. The Verwey transition - a new perspective. *Journal of Physics: Condensed Matter*, 16(7):R145, 2004.

[20] V. L. Ginzburg and L. D. Landau. To the theory of superconductivity. *Zh. Eksp. Teor. Fiz.*, 20:1064.

[21] G. Q. Gong, A. Gupta, Gang Xiao, W. Qian, and V. P. Dravid. Magnetoresistance and magnetic properties of epitaxial magnetite thin films. *Phys. Rev. B*, 56:5096–5099, Sep 1997. doi: 10.1103/PhysRevB.56.5096.

[22] Harold R. Harrison and Ricardo Aragón. Skull melter growth of magnetite (Fe_3O_4). *Materials Research Bulletin*, 13(11):1097 – 1104, 1978. ISSN 0025-5408.

[23] Z. Švindrych, Z. Janů, A. Kozłowski, and J. M. Honig. Low-temperature magnetic anomaly in magnetite. *Phys. Rev. B*, 86:214406, Dec 2012.

[24] Z. Janů, R. Tichý, F. Soukup, M. Novák, and M. Behenský. SQUID magnetometer for HTSC studies with $100\Phi_0 Hz^{-1/2}$ sensitivity continually operating in ± 28 mT AC field. *Czechoslovak Journal of Physics*, 46.

[25] Zdeněk Janů, Jan Hadač, and Zdeněk Švindrych. Glass-like and Verwey transitions in magnetite in details. *Journal of Magnetism and Magnetic Materials*, 310(2, Part 1):e203 – e205, 2007. ISSN 0304-8853.

[26] B. D. Josephson. Possible new effects in superconductive tunnelling. *Physics Letters*, 1(7):251 – 253, 1962. ISSN 0031-9163.

[27] B. D. Josephson. The discovery of tunnelling supercurrents. *Rev. Mod. Phys.*, 46:251–254, Apr 1974.

[28] Z. Kąkol and J. M. Honig. Influence of deviations from ideal stoichiometry on the anisotropy parameters of magnetite Fe_3O_4. *Phys. Rev. B*, 40:9090–9097, Nov 1989.

[29] Takeshi Kasama, Nathan S. Church, Joshua M. Feinberg, Rafael E. Dunin-Borkowski, and Richard J. Harrison. Direct observation of ferrimagnetic/ferroelastic domain interactions in magnetite below the Verwey transition. *Earth and Planetary Science Letters*, 297:10–17, 2010.

[30] K. Kato and Iida S. *Journal of the Physical Society of Japan*, 50(0):2844, 1981.

[31] E. Klugmann. An automatic system for the measurement of magnetic after-effects. *Journal of Physics E: Scientific Instruments*, 13(5):500, 1980.

[32] Masakazu Kobayashi, Yukikuni Akishige, and Etsuro Sawaguchi. Dielectric and conducting properties of single crystal of magnetite below the Verwey point. *Journal of the Physical Society of Japan*, 55(11):4044–4052, 1986.

[33] Abe Kōki, Miyamoto Yoshiko, and Chikazumi Sōshin. Magnetocrystalline anisotropy of low temperature phase of magnetite. *Journal of the Physical Society of Japan*, 41(6):1894–1902, 1976.

[34] A. Kozłowski, Z. Kąkol, D. Kim, R. Zalecki, and J. M. Honig. Heat capacity of $Fe_{3-\alpha}M_\alpha O_4$ (M=Zn, Ti, $0 < \alpha < 0.04$). *Phys. Rev. B*, 54:12093–12098, Nov 1996.

[35] A. Kozłowski, P. Metcalf, Z. Kąkol, and J. M. Honig. Electrical and magnetic properties of $Fe_{3-z}Al_zO_4$ ($z < 0.06$). *Phys. Rev. B*, 53:15113–15118, Jun 1996.

[36] G. Krol, J. Kusz, Z. Tarnawski, Z. Kąkol, A. Kozłowski, and J.M. Honig. Studies of magnetic axis switching phenomenon in magnetite. *Journal of Alloys and Compounds*, 442(1-2):83 – 85, 2007. ISSN 0925-8388.

[37] H. Kronmuller. Theory of magnetic after-effect by valency fluctuations in magnetite. *Journal of Magnetism and Magnetic Materials*, 4(1-4):280 – 286, 1977. ISSN 0304-8853.

[38] Jiwon Lee, Tetsuhiko Isobe, and Mamoru Senna. Preparation of ultrafine Fe_3O_4 particles by precipitation in the presence of PVA at high pH. *Journal of Colloid and Interface Science*, 177(2):490 – 494, 1996. ISSN 0021-9797.

[39] B. Lewis and R. Street. The interpretation of magnetic susceptibility and the ΔE effect in terms of domain processes. *Proceedings of the Physical Society*, 72(4):604, 1958.

[40] D. M. Lind, S. D. Berry, G. Chern, H. Mathias, and L. R. Testardi. Growth and structural characterization of Fe_3O_4 and NiO thin films and superlattices grown by oxygen-plasma-assisted molecular-beam epitaxy. *Phys. Rev. B*, 45: 1838–1850, Jan 1992. doi: 10.1103/PhysRevB.45.1838.

[41] Jianjun Liu, Chun-Gang Duan, Wei-Guo Yin, W. N. Mei, R. W. Smith, and J. R. Hardy. Large dielectric constant and Maxwell-Wagner relaxation in $Bi_{2/3}Cu_3Ti_4O_{12}$. *Phys. Rev. B*, 70:144106, Oct 2004.

[42] A. R. Long. Frequency-dependent loss in amorphous semiconductors. *Advances in Physics*, 31(5):553–637, 1982.

[43] D. E. Mack, S. Wissmann, and K. D. Becker. High-temperature Mossbauer spectroscopy of electronic disorder in complex oxides. *Solid State Ionics*, 135 (1-4):625 – 630, 2000. ISSN 0167-2738.

[44] D. T. Margulies, F. T. Parker, F. E. Spada, R. S. Goldman, J. Li, R. Sinclair, and A. E. Berkowitz. Anomalous moment and anisotropy behavior in Fe_3O_4 films. *Phys. Rev. B*, 53:9175–9187, Apr 1996. doi: 10.1103/PhysRevB.53.9175.

[45] T. Mathews and K. T. Jacob. Seebeck coefficient of magnetite: A reinterpretation invoking Jahn-Teller entropy. *Solid State Communications*, 84(10): 975 – 978, 1992. ISSN 0038-1098.

[46] C. Medrano, M. Schlenker, J. Baruchel, J. Espeso, and Y. Miyamoto. Domains in the low-temperature phase of magnetite from synchrotron-radiation x-ray topographs. *Phys. Rev. B*, 59:1185–1195, Jan 1999.

[47] Russell W. Millar. The heat capacities at low temperatures of "ferrous oxide," magnetite and cuprous and cupric oxides. *Journal of the American Chemical Society*, 51(1):215–222, 1929. doi: 10.1021/ja01376a026.

[48] N. F. Mott. On the transition to metallic conduction in semiconductors. *Canadian Journal of Physics*, 34(12A):1356–1368, 1956.

[49] N. F. Mott. Metal-insulator transition. *Rev. Mod. Phys.*, 40:677–683, Oct 1968.

[50] N. F. Mott. Conduction in non-crystalline materials. *Philosophica Magazine*, 19:835–852, 1969.

[51] A. R. Muxworthy and E. McClelland. Review of the low-temperature magnetic properties of magnetite from a rock magnetic perspective. *Geophysical Journal International*, 140(1):101–114, 2000. ISSN 1365-246X.

[52] P. Novak, H. Stepankova, J. Englich, J. Kohout, and V. A. M. Brabers. NMR in magnetite below and around the Verwey transition. *Physical Review B*, 61(2):1256, 2000.

[53] Ozden Ozdemir and David J. Dunlop. Low-temperature properties of a single crystal of magnetite oriented along principal magnetic axes. *Earth and Planetary Science Letters*, 165(2):229 – 239, 1999. ISSN 0012-821X.

[54] Wilfred Palmer. Magnetocrystalline anisotropy of magnetite at low temperature. *Phys. Rev.*, 131:1057–1062, Aug 1963.

[55] G. S. Parks and K. K. Kelley. The heat capacities of some metallic oxides. *The Journal of Physical Chemistry*, 30(1):47–55, 1925. doi: 10.1021/j150259a005.

[56] M. Pollak and T. H. Geballe. Low-frequency conductivity due to hopping processes in silicon. *Phys. Rev.*, 122:1742–1753, Jun 1961.

[57] S. C. Qu, H. B. Yang, D. W. Ren, S. H. Kan, G. T. Zou, D. M. Li, and M. H. Li. Magnetite nanoparticles prepared by precipitation from partially reduced ferric chloride aqueous solutions. *Journal of Colloid and Interface Scinece*, 215(1):190–192, Jul 1999.

[58] G. T. Rado and J. M. Ferrari. Electric field dependence of magnetic anisotropy energy in magnetite. *Physical Review B*, 12(11):5166, 1975.

[59] H. J. Reichmann and S. D. Jacobsen. High-pressure elasticity of a natural magnetite crystal. *American Mineralogist*, 89(7):1061–1066, 2004.

[60] G. Kh. Rozenberg, Y. Amiel, W. M. Xu, M. P. Pasternak, R. Jeanloz, M. Hanfland, and R. D. Taylor. Structural characterization of temperature- and pressure-induced inverse↔normal spinel transformation in magnetite. *Phys. Rev. B*, 75:020102, Jan 2007.

[61] Gregory Kh. Rozenberg, Giovanni R. Hearne, Moshe P. Pasternak, P. A. Metcalf, and J. M. Honig. Nature of the Verwey transition in magnetite (Fe_3O_4) to pressures of 16 GPa. *Phys. Rev. B*, 53:6482–6487, Mar 1996.

[62] T. Schrefl, J. Fidler, and H. Kronmüller. Remanence and coercivity in isotropic nanocrystalline permanent magnets. *Phys. Rev. B*, 49:6100–6110, Mar 1994. doi: 10.1103/PhysRevB.49.6100.

[63] Mark S. Senn, Jon P. Wright, and J. Paul Attfield. Charge order and three-site distortions in the Verwey structure of magnetite. *Nature*, 481(0):173–176, 2012.

[64] Z. Simsa, F. Zounova, and S. Krupicka. Initial permeabilty of single crystal magnetite and Mn-ferrite. *Czechoslovak Journal of Physics*, B35(0):1271, 1985.

[65] Ralph Skomski. *Introduction: The simplest models of magnetism*. Oxford University Press, 2008. ISBN 978-0198570752. doi: 10.1093/acprof:oso/9780198570752.001.0001.

[66] J. L. Snoek. Time effects in magnetization. *Physica*, 5(8):663 – 688, 1938. ISSN 0031-8914.

[67] J. L. Snoek. Magnetic aftereffect and chemical constitution. *Physica*, 6(2): 161 – 170, 1939. ISSN 0031-8914.

[68] J. Spałek, A. Kozłowski, Z. Tarnawski, Z. Kąkol, Y. Fukami, F. Ono, R. Zach, L. J. Spałek, and J. M. Honig. Verwey transition in Fe_3O_4 at high pressure: Quantum critical point at the onset of metallization. *Phys. Rev. B*, 78: 100401, Sep 2008.

[69] E. J. W. Verwey. *Nature*, 144:327, 1939.

[70] F. Walz. Ein automatisiertes meßverfahren zur bestimmung der magnetischen nachwirkung in ferromagnetika. *Physica Status Solidi (a)*, 8(1):125–133, 1971. ISSN 1521-396X.

[71] F. Walz and H. Kronműller. Analysis of magnetic point-defect relaxations in electron-irradiated magnetite. *Physica Status Solidi (b)*, 181(2):485–498, 1994. ISSN 1521-3951.

[72] F. Walz, M. Weidner, and H. Kronműller. Investigation of magnetic after-effects in magnetite at low temperatures (4 to 35 K). *Physica Status Solidi (a)*, 59(1):171–182, 1980. ISSN 1521-396X.

[73] F. Walz, V. A. M. Brabers, S. Chikazumi, H. Kronműller, and M. O. Rigo. Magnetic after-effects in single- and poly-crystalline magnetite. *Physica Status Solidi (b)*, 110(2):471–478, 1982. ISSN 1521-3951.

[74] F. Walz, V. A. M Brabers, J. H. V. J. Brabers, and H Kronmuller. Timescale settling and nature of electron transport in magnetite – general considerations in view of new magnetic after-effect results on dilutely Ti^{4+}-doped Fe_3O_4. *Journal of Physics: Condensed Matter*, 17(42):6763, 2005.

[75] Friedrich Walz. The Verwey transition - a topical review. *Journal of Physics: Condensed Matter*, 14(12):R285–R340, 2002.

[76] Pierre Weiss and Karl Renger. Die anfangliche permeabilitat von eisen und magnetit in funktion der temperatur und die abhangigkeit der umwandlungspunkte von der feldstarke. *Electrical Engineering (Archiv fur Elektrotechnik)*, 2:406–418, 1914. ISSN 0948-7921.

[77] M. Ziese, R. Höhne, P. Esquinazi, and P. Busch. Micromagnetic studies of magnetite films using μ-hall sensor arrays. *Phys. Rev. B*, 66:134408, Oct 2002.

[78] J. M. Zuo, J. C. H. Spence, and W. Petuskey. Charge ordering in magnetite at low temperatures. *Phys. Rev. B*, 42:8451–8464, Nov 1990.

Author's publications and presentations

Zdeněk Švindrych, Zdeněk Janů, Andrzej Kozłowski, Jurgen M. Honig, *Low-temperature magnetic anomaly in magnetite*, Physical Review B **86** (2012) 214406, DOI: 10.1103 / PhysRevB.86.214406

Zdeněk Janů, Zdeněk Švindrych, Ahmed Youssef, Lucia Baničová, *Critical state analysis using continuous reading SQUID magnetometer*, Chapter 12 in book: Superconductivity - Theory and Applications, ed. by Adir Moyses Luiz, InTech 2011, ISBN 978-953-307-151-0, DOI: 10.5772/684

Zdeněk Švindrych, Ahmed Youssef, Zdeněk Janů, *Link between Magnetic and Dielectric Properties in Magnetite*, Acta Physica Polonica A **118** (2010) 940-941

Zdeněk Janů, Jan Hadač, Zdeněk Švindrych, *Glass-like and Verwey transitions in magnetite in details*, Journal of Magnetism and Magnetic Materials **310** (2007) e203-e205, DOI: 10.1016 / j.jmmm.2006.10.344

Zdeněk Janů, Zdeněk Švindrych, Otakar Truněček, Peter Kús, Andrej Plecenik, *AC susceptibility of thin Pb films in intermediate and mixed state*, Physica C: Superconductivity and its Applications **471** (2011) 1647-1650, DOI: 10.1016 / j.physc.2011.07.010

Ahmed Youssef, Zdeněk Švindrych, Zdeněk Janů, *Analysis of magnetic response of critical state in second-generation high temperature superconductor* $YBa_2Cu_3O_x$ *wire*, Journal of Applied Physics **106** (2009) 063901, DOI: 10.1063/1.3222850

Ahmed Youssef, Zdeněk Švindrych, Jan Hadač, Zdeněk Janů, *Analysis of critical state response in thin films by AC susceptibility measurements*, IEEE Transactions on Applied Superconductivity **18** (2008) 1589-1592,
DOI: 10.1109 / TASC.2008.922391

Ahmed Youssef, Lucia Baničová, Zdeněk Švindrych, Zdeněk Janů, *Contactless Estimation of Critical Current Density and Its Temperature Dependence Using Magnetic Measurements*, Acta Physica Polonica A **118** (2010) 1036-1037

Zdeněk Švindrych, Zdeněk Janů, František Soukup, Rudolf Tichý, *Operational amplifiers operating in temperature range from 300 to 4.2 K*, Cryogenics **48** (2008) 160-165, DOI: 10.1016 / j.cryogenics.2008.03.009

List of Symbols and Abbreviations

$\mathbf{A}$	magnetic vector potential
a.u.	arbitrary units
$\mathbf{B}$	magnetic induction
C	electric capacitance
c	speed of light
χ	magnetic susceptibility
χ_{ac}	complex ac magnetic susceptibility
χ'	real part of ac magnetic susceptibility
χ''	imaginary part of ac magnetic susceptibility
χ_n	n^{th} harmonic of complex ac magnetic susceptibility
χ'_n	real part of n^{th} harmonic of ac magnetic susceptibility
χ''_n	imaginary part of n^{th} harmonic of ac magnetic susceptibility
$\mathbf{D}$	electric induction
D	demagnetising factor
δ	magnetite sample nonstoichiometry - $Fe_{3(1-\delta)}O_4$
$\mathbf{E}$	electric field intensity
E	energy
E_a	activation energy in exponential models of thermal activation
e	absolute value of electron charge
ε	dielectric permittivity
ε_0	vacuum dielectric permittivity
$\mathbf{F}$	force
f	frequency
$\mathscr{F}$	Fourier transform
$\mathbf{H}$	magnetic field intensity
H_a	externally applied magnetic field
H_{ac}	amplitude of harmonic component of magnetic field
H_{dc}	dc component of magnetic field
$\hbar$	reduced Planck's constant
K	anisotropy constant
k_B	Botzmann constant
L	electric inductance
$\mathbf{M}$	magnetisation
M_s	saturated magnteisation
$\mathbf{m}$	magnetic moment
MAE	Magnetic After-Effect
m	mass
μ	magnetic permeability
μ_0	vacuum magnetic permeability
μ_B	Bohr magnetron
N_A	Avogadro number
NMR	Nuclear Magnetic Resonance

Continued on next page...

ω	angular frequency
p	pressure
Φ	magnetic flux
Φ_0	quantum of magnetic flux (about $2.07 \cdot 10^{-15}$ Wb)
π	ratio of circle circumference to its radius
R	electric resistance
ρ	electric resistivity
ϱ	mass density
SQUID	Superconducting QUantum Interference Device
σ	electric conductivity
T	absolute temperature
T_a	magnetic-anomaly transition temperature
T_g	"glass" transition temperature
T_V	Verwey temperature
t	time
τ	relaxation time, torque
V	volume
Z	electric impedance
ZFC	Zero Field Cooled